# The histone demethylase UTX regulates the lineage-specific epigenetic program of invariant natural killer T cells

Semir Beyaz[1,2,9], Ji Hyung Kim[3,9], Luca Pinello[4,9], Michael E Xifaras[5], Yu Hu[3], Jialiang Huang[4], Marc A Kerenyi[1,2,6], Partha P Das[1,2], R Anthony Barnitz[1,7], Aurelie Herault[8], Rizkullah Dogum[5], W Nicholas Haining[1,7], Ömer H Yilmaz[5], Emmanuelle Passegue[8], Guo-Cheng Yuan[4], Stuart H Orkin[1,2,10] & Florian Winau[3,10]

Invariant natural killer T cells (*i*NKT cells) are innate-like lymphocytes that protect against infection, autoimmune disease and cancer. However, little is known about the epigenetic regulation of *i*NKT cell development. Here we found that the H3K27me3 histone demethylase UTX was an essential cell-intrinsic factor that controlled an *i*NKT-cell lineage-specific gene-expression program and epigenetic landscape in a demethylase-activity-dependent manner. UTX-deficient *i*NKT cells exhibited impaired expression of *i*NKT cell signature genes due to a decrease in activation-associated H3K4me3 marks and an increase in repressive H3K27me3 marks within the promoters occupied by UTX. We found that JunB regulated *i*NKT cell development and that the expression of genes that were targets of both JunB and the *i*NKT cell master transcription factor PLZF was UTX dependent. We identified *i*NKT cell super-enhancers and demonstrated that UTX-mediated regulation of super-enhancer accessibility was a key mechanism for commitment to the *i*NKT cell lineage. Our findings reveal how UTX regulates the development of *i*NKT cells through multiple epigenetic mechanisms.

Invariant natural killer T cells (*i*NKT cells) are a subset of T lymphocytes with a limited T cell antigen receptor (TCR) repertoire that recognizes lipid antigens presented by CD1d molecules on the surface of antigen-presenting cells[1,2]. The prototypical lipid antigen is the glycosphingolipid α-galactosylceramide derived from a marine sponge[3], which can be loaded onto CD1d tetramers for the detection of *i*NKT cells through binding to their invariant TCR. Following antigen recognition, *i*NKT cells respond rapidly in an innate-like fashion and secrete inflammatory cytokines, including interferon-γ (IFN-γ) and interleukin 4 (IL-4), in copious amounts[1,2]. This early response influences the outcome of downstream immunological reactions and endows *i*NKT cells with regulatory properties. Due to the diversity of their effector functions, *i*NKT cells are involved in many pathological processes. Accordingly, they are important in host defense against infections, prevent autoimmune disorders and protect against cancer[1,4].

Delineating the molecular mechanisms that control specification to the *i*NKT cell lineage is essential for the development of potential therapeutic applications that target *i*NKT cells. Commitment to the *i*NKT cell lineage involves positive selection of precursors of *i*NKT cells by CD4+CD8+ double-positive (DP) thymocytes that express CD1d-glycolipid complexes[5]. After positive selection, TCR signaling activates a pathway of calcineurin and the transcription factor NFAT that induces expression of the transcription factor Egr2 (ref. 6). Following that induction, Egr2 activates the *i*NKT cell master regulator PLZF (encoded by *Zbtb16*) and the common β-subunit of the IL-2–IL-15 receptor (CD122; encoded by *Il2rb*), which leads to the subsequent steps of *i*NKT cell development, composed of cytokine expression and proliferation in response to the IL-15–CD122 axis[7–10]. T-bet (encoded by *Tbx21*) is a key transcription factor that regulates the differentiation of *i*NKT cells and their acquisition of NK cell traits during terminal maturation. After egressing from the thymus, *i*NKT cells reside mainly in the liver and spleen to perform their effector functions[11]. Although published reports have contributed to an understanding of how key transcription factors establish *i*NKT

[1]Division of Hematology/Oncology, Boston Children's Hospital, Harvard Medical School, Boston, Massachusetts, USA. [2]Department of Pediatric Oncology, Dana-Farber Cancer Institute, Howard Hughes Medical Institute, Harvard Stem Cell Institute, Harvard Medical School, Boston, Massachusetts, USA. [3]Program in Cellular and Molecular Medicine, Boston Children's Hospital, Harvard Medical School, Boston, Massachusetts, USA, and Department of Microbiology and Immunobiology, Harvard Medical School, Boston, Massachusetts, USA. [4]Department of Biostatistics and Computational Biology, Dana-Farber Cancer Institute, Boston, Massachusetts, USA, and Harvard T.H. Chan School of Public Health, Boston, Massachusetts, USA. [5]The David H. Koch Institute for Integrative Cancer Research at MIT, Cambridge, Massachusetts, USA, and Department of Biology, Massachusetts Institute of Technology, Cambridge, Massachusetts, USA. [6]Department of Pharmacology and Translational Research, Boehringer Ingelheim, Vienna, Austria. [7]Department of Pediatric Oncology, Dana-Farber Cancer Institute, Broad Institute of MIT and Harvard, Cambridge, USA. [8]The Eli and Edythe Broad Center for Regenerative Medicine and Stem Cell Research, University of California San Francisco, California, USA, and Department of Medicine, Division of Hematology/Oncology, University of California San Francisco, San Francisco, California, USA. [9]These authors contributed equally to this work. [10]These authors jointly directed this work. Correspondence should be addressed to S.H.O (stuart_orkin@dfci.harvard.edu) or F.W. (florian.winau@childrens.harvard.edu).

Received 12 September; accepted 23 November; published online 19 December 2016; doi:10.1038/ni.3644

cell identity in a stepwise process[12,13], it is unclear how a multitude of transcription factors are orchestrated within an epigenetic framework that controls lineage-specific gene expression in *i*NKT cells.

During development, cell-fate determination relies on the activation of cell-type-restricted transcription factors that act at promoters and enhancers of genes. This requires epigenetic programming to ensure the establishment of proper chromatin organization. Stretch-enhancer elements ('super-enhancers') have a critical role in the control of cell identity[14,15]. Dynamic regulation of the histone-methylation state at promoters or enhancers by histone-modifying enzymes is a key epigenetic mechanism that affects lineage-specific gene expression[16–18]. The polycomb repressive complex PRC2 catalyzes the trimethylation of histone H3 on lysine 27 (to produce H3K27me3) that is associated with poised or repressed states of promoters and enhancers[17,19,20]. In contrast, demethylation of H3K27me3 by the histone demethylases UTX and JMJD3 correlates with active chromatin states that facilitate gene expression[21–25]. UTX and JMJD3 serve important roles in early development[21–23,26], epigenetic reprogramming[27], cellular differentiation[24,28–30] and cancer[31,32]. The role of UTX in various T lymphocyte subsets has been addressed[33–35]; however, the underlying mechanisms of its effects remain to be elucidated.

In this study, we assessed the epigenetic mechanisms by which UTX controls the development of *i*NKT cells. Deficiency in UTX resulted in the downregulation of *i*NKT cell signature genes, including *Tbx21*, *Il2rb* and *Klrd1*, and blocked *i*NKT cell development. We demonstrated that the abundance of H3K27me3 was greater and that of H3K4me3 was lower around the promoters of downregulated signature genes in UTX-deficient *i*NKT cells than in UTX-sufficient *i*NKT cells. We found that UTX partnered with PLZF, and that UTX-deficient *i*NKT cells failed to activate PLZF target genes and harbored more H3K27me3 around their gene promoters than did UTX-sufficient *i*NKT cells. Moreover, we discovered a role for the AP-1 transcription factor JunB in the generation of *i*NKT cells. By delineating the super-enhancer landscape of *i*NKT cells, we demonstrated that UTX was required for the accessibility of the super-enhancers of genes encoding products that mediate specification to the *i*NKT cell lineage. Thus, we found that UTX engaged multiple gene-regulatory mechanisms to facilitate the lineage-specific gene expression and development of *i*NKT cells.

## RESULTS

### Requirement for UTX in *i*NKT cell development

Initially, we assessed the requirements for UTX and JMJD3 broadly in the hematopoietic system. For this purpose, we generated mice with *lox*P-flanked alleles encoding UTX or JMJD3, then interbred those with mice expressing Cre recombinase from the *Vav* allele for conditional gene inactivation in the adult hematopoietic system, to generate mice with such conditional deficiency in UTX (UTX-KO) or JMJD3 (JMJD3-KO) (**Supplementary Fig. 1a**–**e**). We observed that the number of *i*NKT cells was much lower in the thymus, spleen and liver of UTX-KO or JMJD3-KO mice than in that of UTX- and JMJD3-sufficient mice (which served as controls throughout), with a more pronounced effect for mice with UTX deficiency (**Fig. 1a**). Mice with deficiency of both UTX and JMJD3 in the adult hematopoietic system (DKO mice) had a phenotype similar to that of UTX-KO mice (**Fig. 1a**), which suggested that ablation of JMJD3 had no additive effects. We confirmed the deletion of transcripts encoding UTX or JMJD3 in the blood, DP thymocytes and *i*NKT cells of UTX-KO or JMJD3-KO mice, respectively, by quantitative PCR (**Supplementary Fig. 1f**). Through the use of molecular markers to distinguish the stages of *i*NKT cell development[36], analysis of the remaining thymic *i*NKT cells in UTX-KO or JMJD3-KO mice revealed a maturation block that prevented *i*NKT

cells from fully entering into stage 3, with relative accumulation in stages 1 and 2 (**Fig. 1b**–**d**). These results indicated a selective role for UTX and JMJD3 in *i*NKT cells during blood-cell differentiation. Since the altered *i*NKT cell phenotype proved to be predominant in UTX deficiency, we focused our subsequent analyses on UTX.

Next we assessed the influence of loss of UTX on the functional properties of *i*NKT cells. After stimulation with α-galactosylceramide, IFN-γ production was lower in thymic *i*NKT cells of UTX-KO mice than in those of control mice (**Supplementary Fig. 2a**), reflective of a lack of fully mature cells. However, the synthesis of IL-4 in the thymus and production of IFN-γ by the few remaining liver *i*NKT cells in UTX-KO mice was unaltered relative to that in control mice (**Supplementary Fig. 2a**). A published classification, although not mutually exclusive with the maturation model, has categorized *i*NKT cell development into the subtypes 'NKT1', 'NKT2' and 'NKT17' on the basis of cytokine profile and specific transcription factors[37]. We observed considerably fewer T-bet-dependent NKT1 cells in UTX-deficient mice than in control mice (**Supplementary Fig. 2b**). To exclude the possibility that the impaired development of *i*NKT cells was a consequence of failure of antigen presentation or rearrangement of the $V_{\alpha}14$-$J_{\alpha}18$ TCR, we demonstrated equivalent expression of CD1d and abundance of transcripts encoding $V_{\alpha}14$-$J_{\alpha}18$ in UTX-deficient DP thymocytes and control DP thymocytes (**Supplementary Fig. 2c,d**). Thus, UTX did not affect mainly the function of *i*NKT cells but instead affected mainly their development.

### Control of *i*NKT-cell-lineage-specific gene expression by UTX

To elucidate the molecular mechanism by which UTX contributed to the development of *i*NKT cells, we sorted thymic *i*NKT cells from UTX-KO or control mice and performed gene-expression analysis (**Supplementary Fig. 3a**). Genes downregulated in UTX-KO *i*NKT cells relative to their expression in control *i*NKT cells comprised those induced during *i*NKT cell maturation and included those encoding the critical transcription factor T-bet (*Tbx21*)[11], the NK cell receptor NKG2D (*Klrk1*), the chemokine and cytokine receptors CXCR3 (*Cxcr3*) and CD122 (*Il2rb*)[9], as well as the cytokine IFN-γ (*Ifng*) and the calcium regulator calcyclin (*S100a6*)[13] (**Fig. 2a**). Gene-set–enrichment analysis (GSEA) of the genes downregulated in UTX-deficient *i*NKT cells revealed enrichment, among the downregulated genes, for genes encoding products involved in *i*NKT cell differentiation as well as in signaling pathways, including IL-12 and NFAT, which have been reported to have important roles in *i*NKT cells[6,13] (**Fig. 2b** and **Supplementary Fig. 3b**). Using quantitative PCR, we confirmed the expression of a subset of signature genes whose downregulation depended on UTX and observed substantial downregulation of *Tbx21*, *S100a6*, *Klrd1* and *Klrk1* (which encode NK cell receptors), *Cxcr3* and *Il2rb* in UTX-deficient thymic *i*NKT cells relative to their expression in control thymic *i*NKT cells (**Fig. 2c**). Correspondingly, *i*NKT cells from UTX-KO mice had lower protein expression of the products of those genes than that of *i*NKT cells from control mice (**Fig. 2d**). In contrast, UTX deficiency resulted in the upregulation of genes encoding products involved in the cell-cycle, DNA-replication and DNA-repair pathways (**Supplementary Fig. 3c**). We confirmed loss of transcripts encoding UTX and UTX-dependent downregulation of signature genes in UTX-KO *i*NKT cells at various stages of development (**Supplementary Fig. 3d**,**e**). These findings indicated that *i*NKT cell development required a UTX-mediated lineage-specific gene-expression program.

### Regulation of the epigenetic landscape of *i*NKT cells by UTX

UTX-mediated demethylation of H3K27me3 and concomitant catalysis of the trimethylation of H3K4 by the methyltransferase
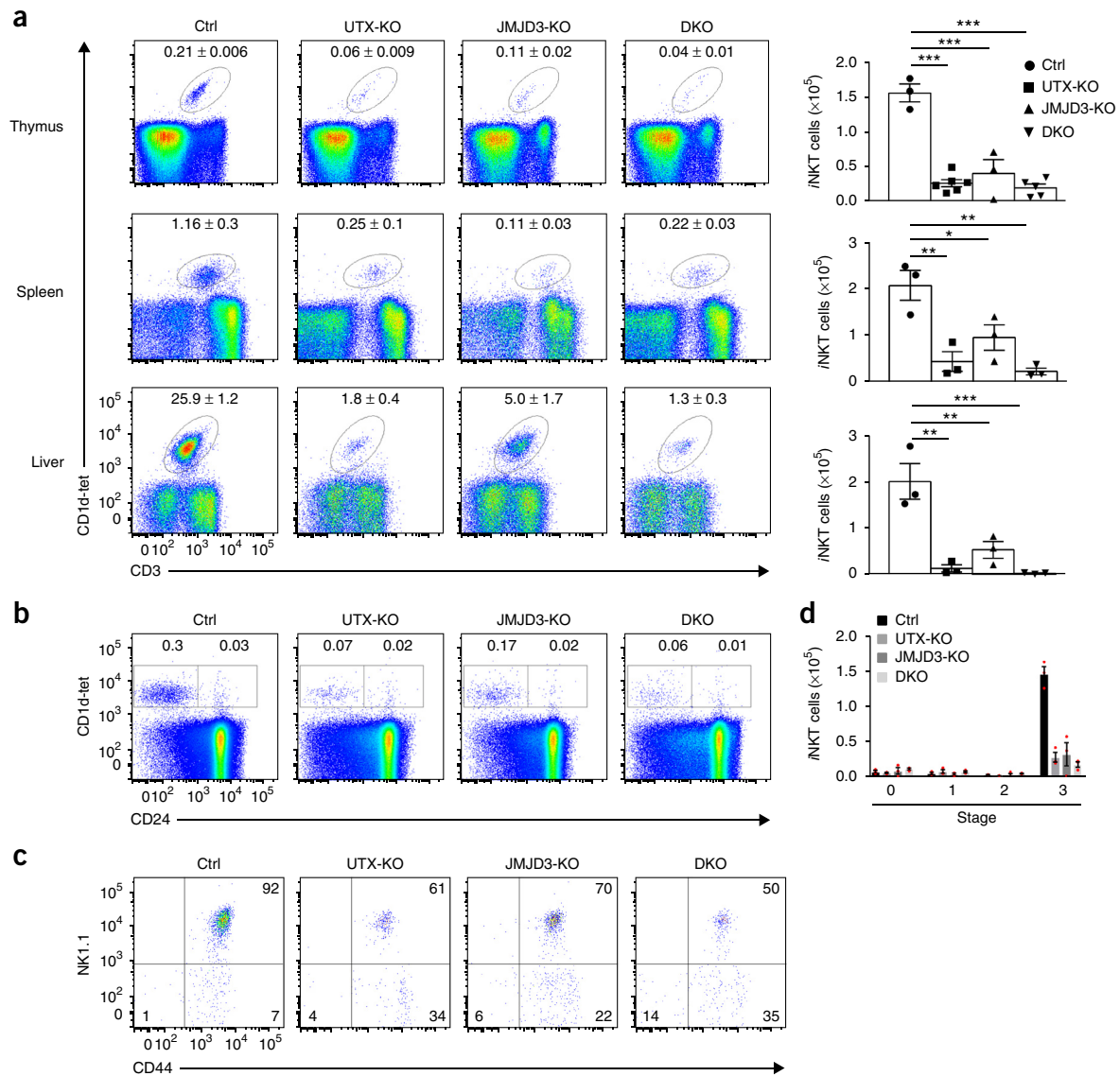
**Figure 1** H3K27 demethylases are essential for the maturation and development of *i*NKT cells. (**a**) Flow cytometry (left) of *i*NKT cells from the thymus, spleen and liver (left margin) of UTX-sufficient (control) mice (Ctrl; $n = 3$), UTX-KO mice ($n = 6$ (thymus) or $n = 3$ (spleen and liver)), JMJD3-KO mice ($n = 3$) and DKO mice ($n = 5$ (thymus) or $n = 3$ (liver and spleen)), detected by staining with antibody to the TCR invariant chain CD3 (anti-CD3) and α-galactosylceramide-loaded CD1d tetramers (CD1d-tet); right, absolute number of *i*NKT cells in mice as at left. Numbers above outlined areas (left) indicate percent CD1d-tet⁺CD3⁺ *i*NKT cells (mean ± s.e.m.). (**b**) Flow cytometry of *i*NKT cells from mice as in **a** ($n = 4$ per group). Numbers above outlined areas indicate percent CD1d-tet⁺CD24⁺ cells (stage 0; right) or CD1d-tet⁺CD24⁻ cells (stages 1–3; left). (**c**) Expression of NK1.1 and CD44 by thymic *i*NKT cells as in **b** (gated as CD1d-tet⁺CD24⁻). Numbers in quadrants indicate percent NK1.1⁻CD44⁻ cells (stage 1; bottom left), NK1.1⁻CD44⁺ cells (stage 2; bottom right) or NK1.1⁺CD44⁺ cells (stage 3; top right). (**d**) Absolute number of thymic *i*NKT cells as in **b,c**. Each symbol (**a,d**) represents an individual mouse. *$P < 0.05$, **$P < 0.01$ and ***$P < 0.001$ (one-way analysis of variance (ANOVA) and multiple comparisons). Data are from three independent experiments (mean ± s.e.m. in **a,d**).

MLL2 around gene promoters correlates with active gene expression[23]. Therefore, we hypothesized that during *i*NKT cell development, transcriptional activation of genes specific to the *i*NKT cell lineage involves UTX-dependent chromatin regulation. To address this hypothesis, we examined the epigenetic landscape of *i*NKT cells from UTX-KO or control thymi by genome-wide chromatin immunoprecipitation followed by deep sequencing (ChIP-Seq) for H3K4me3 marks and H3K27me3 marks, which correlate with activation or repression, respectively. We applied a model-based analysis of ChIP-Seq (MACS2) to identify distinct peaks in each condition. Although genome-wide H3K4me3 peaks were largely shared by control *i*NKT cells and UTX-KO *i*NKT cells (**Fig. 3a**), genome-wide

H3K27me3 peaks were much more abundant in the absence of UTX (**Fig. 3b**), consistent with the role of UTX in the demethylation of H3K27me3. In addition to that accumulation of global H3K27me3 content in UTX-KO *i*NKT cells (9,645), we observed that some regions exhibited control-cell-specific H3K27me3 peaks (4,250) (**Fig. 3b**). While the chromosomal distribution of control-cell-specific H3K27me3 peaks was similar to that of UTX-KO-cell-specific H3K27me3 peaks (**Supplementary Fig. 4a,b**), control-cell-specific H3K27me3 peaks were more abundant in distal intergenic regions than were UTX-KO-cell-specific peaks (33.5% (control) versus 24.7% (UTX-KO); **Supplementary Fig. 4c,d**). Notably, we detected a greater abundance of UTX-KO-cell-specific H3K27me3 peaks (13.4%) than
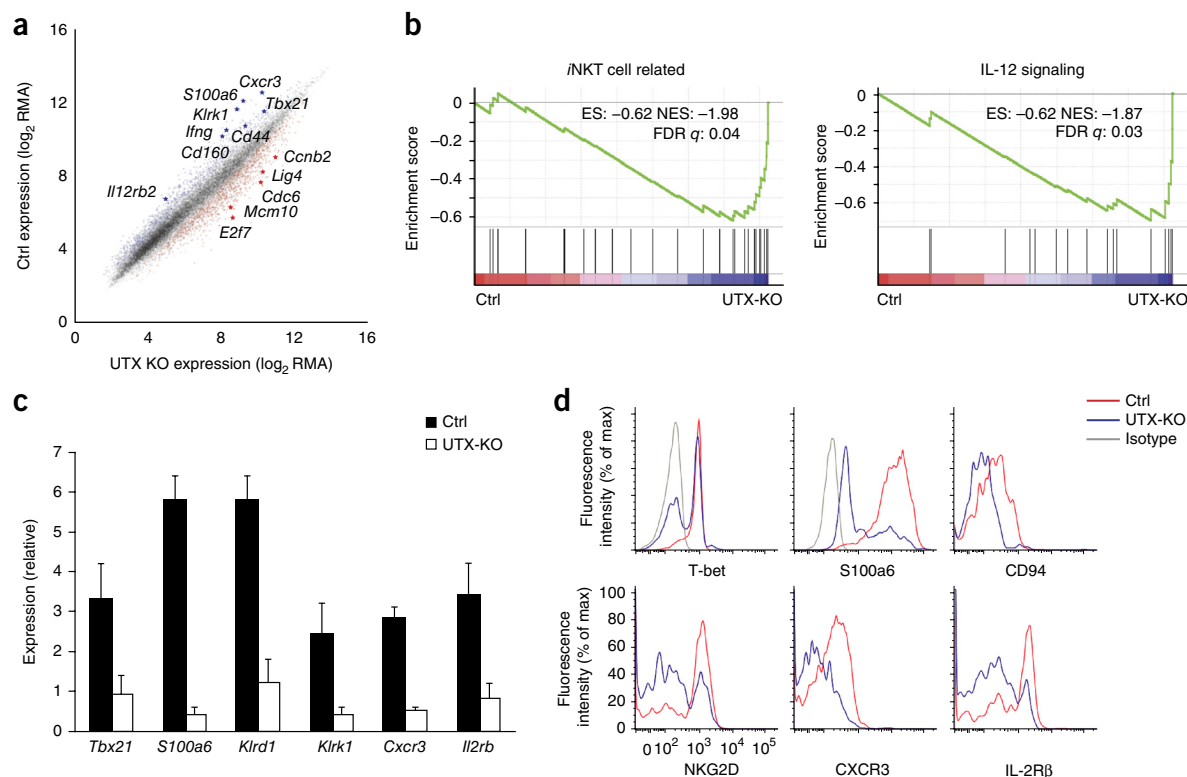
**Figure 2** UTX is required for the lineage-specific expression of signature genes in *i*NKT cell development. (**a**) Gene expression in thymic *i*NKT cells, showing genes upregulated (red) or downregulated (blue) in UTX-KO cells relative to their expression in UTX-sufficient (control) *i*NKT cells; results are presented as robust multi-array average (RMA) (normalized fluorescence units of probes on array). (**b**) Gene-set–enrichment analysis of genes downregulated as in **a**, encoding products related to *i*NKT cells (left) or IL-12 signaling (right); results are presented as enrichment score (ES), normalized enrichment score (NES) and false-discovery rate (FDR). (**c**) Quantitative RT-PCR analysis of genes downregulated as in **a** (horizontal axis); results were normalized to those of the control gene *Actb*. (**d**) Flow cytometry of thymic control or UTX-KO *i*NKT cells (key) gated on CD3+CD1d-tet+ cells and stained for products of genes in the *i*NKT cell expression signature (horizontal axes); results are presented as fluorescence intensity. Isotype, isotype-matched control antibody. Data are from two experiments with five mice (control) or four mice (UTX-KO) (**a,b**), or five independent experiments (**c**; mean + s.d.) or are representative of three independent experiments (**d**).

control-cell-specific H3K27me3 peaks (10.4%) in proximal promoters (**Supplementary Fig. 4c,d**). Analysis with the Genomic Regions Enrichment of Annotations Tool (GREAT) demonstrated that regions with loss of H3K27me3 peaks in UTX-KO *i*NKT cells showed enrichment for bivalent genes with both H3K27me3 and H3K4me3 in their promoters, as well as genes encoding products involved in erythrocyte development (**Supplementary Fig. 5a**). Notably, regions that gained H3K27me3 peaks in UTX deficiency showed enrichment for genes that require MLL for their transcription, as well as genes induced in memory T cells (**Supplementary Fig. 5b**).

Since UTX-mediated alterations to histone marks around promoters affect gene expression, we investigated the average abundance of histone marks at gene promoters in *i*NKT cells (**Fig. 3c–e**). In UTX-KO *i*NKT cells, we observed significant accumulation of H3K27me3 around the transcription start sites (TSSs) and promoters of downregulated genes (**Fig. 3d** and **Supplementary Fig. 5c**). Moreover, we observed a much lower abundance of H3K4me3 in the downregulated genes in UTX-KO *i*NKT cells than in control cells (**Fig. 3d**). While there was less significant accumulation of H3K27me3 around the promoters of upregulated genes than around those of downregulated genes in UTX-KO *i*NKT cells ($P = 9 \times 10^{-4}$ (permutation test); **Supplementary Fig. 5d**), there was no notable difference in the abundance of H3K4me3 in this comparison (**Fig. 3e**). GREAT analysis of the promoter regions of downregulated genes revealed enrichment for genes encoding products involved in *i*NKT cell development

(**Supplementary Fig. 5e**), while similar analysis of upregulated genes demonstrated an association with the cell-cycle and DNA-repair pathways (**Supplementary Fig. 5f**). These results suggested that UTX controlled *i*NKT cell development by regulating the chromatin landscape around the promoters of downregulated genes encoding products involved in *i*NKT cell differentiation.

**Regulation of *i*NKT-cell-signature-gene promoters by UTX**
To identify the various patterns of chromatin state and to explore promoters with substantial UTX-dependent chromatin regulation, we identified clusters on the basis of the distribution of H3K4me3 and H3K27me3 around the promoters of the downregulated (**Fig. 3f–i** and **Supplementary Fig. 6a**) and upregulated genes (**Supplementary Fig. 6b,c**) identified above. For the downregulated genes, cluster 1 included promoters with a similar abundance of H3K4me3 in control *i*NKT cells and UTX-KO *i*NKT cells and a slightly greater abundance of H3K27me3 in the absence of UTX (**Fig. 3f**). Cluster 2 included promoters with a very low abundance of H3K4me3 and similar abundance of H3K27me3 in control *i*NKT cells and UTX-KO *i*NKT cells (**Fig. 3g**). Notably, promoters in cluster 3 (**Fig. 3h**) and cluster 4 (**Fig. 3i**) had a much lower abundance of H3K4me3 and accumulation of H3K27me3, especially around the TSS, which suggested that these promoters were affected by UTX-dependent chromatin regulation. Integration of gene-expression data with chromatin state revealed that the genes most downregulated were in cluster 3 (**Fig. 3h**), which
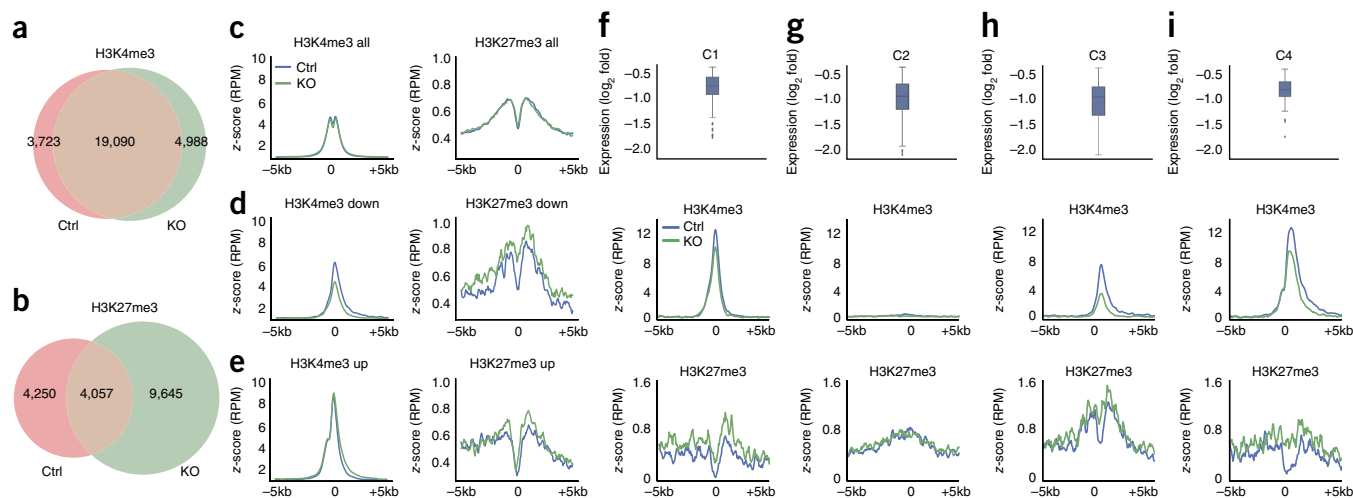
**Figure 3** UTX regulates the chromatin landscape of *i*NKT cells. (**a,b**) Genome-wide peaks of the histone marks H3K4me3 (active) (**a**), and H3K27me3 (repressive) (**b**) in UTX-sufficient (control) and UTX-KO (KO) *i*NKT cells. (**c**–**e**) Abundance of H3K4me3 (left) and H3K27me3 (right) around the promoters of all *i*NKT cell genes (all; **c**), downregulated genes (down; **d**) or upregulated genes (up; **e**) in UTX-KO *i*NKT cells (key); results are presented as average *z*-score in reads per million (RPM). 0, TSS. (**f**–**i**) Integration of gene expression (top row; $\log_2$ fold values) with abundance of H3K4me3 (middle row) or H3K27me3 (bottom row) around gene promoters (presented as in **c**–**e**), for genes downregulated in UTX-KO *i*NKT cells, categorized as clusters C1 (**f**), C2 (**g**), C3 (**h**) and C4 (**i**) according to histone mark pattern. Top row: boxes extend from the lower to upper quartile values; small horizontal line indicates the median (whiskers, 1.5 inter-quartile range, with outliers (symbols) beyond). $P < 1 \times 10^{-5}$ (H3K4me3 and H3K27me3 in **d,h,i**), $P = 0.16$ (H3K4me3 in **e**) or $P = 9 \times 10^{-4}$ (H3K27me3 in **e**) (permutation test with 100,000 permutations). Data are from two independent experiments.

indicated that UTX-mediated removal of H3K27me3 around these promoters was critical for activation of transcription. We identified the promoters in cluster 3 and cluster 4 (**Supplementary Table 1**) with significant UTX-dependent chromatin regulation by GREAT analysis. We found that cluster 3 and cluster 4 showed significant enrichment for genes encoding products involved in the immune response and signature genes encoding products involved in *i*NKT cell differentiation (the '*Klr*' family, *Cxcr3* and *S100a6* (cluster 3) and *Tbx21* (cluster 4); **Supplementary Fig. 6d**). Cluster analysis of the upregulated genes showed that the abundance of H3K4me3 and H3K27me3 was largely similar in UTX-KO *i*NKT cells and control *i*NKT cells (**Supplementary Fig. 6b,c**). These results emphasized that deficiency in UTX affected the chromatin state specifically around the promoters of a subset of downregulated genes, which constituted the *i*NKT cell signature in cluster 3 and cluster 4, without a robust effect on the chromatin state of other genes.

### Binding of UTX to *i*NKT-cell-signature-gene promoters

To assess specific alterations in the abundance of H3K4me3 and H3K27me3 around the promoters of genes with UTX-dependent transcriptional and chromatin regulation, we generated overlay tracks of ChIP-Seq data from control and UTX-KO *i*NKT cells using the Integrative Genomics Viewer visualization tool. We found a much lower abundance of H3K4me3 and an accumulation of H3K27me3 around the promoters of the signature genes *S100a6*, *Il2rb*, *Klrd1*, *Klrk1*, *Cxcr3* and *Tbx21* in UTX-KO *i*NKT cells relative to their abundance at those genes in control cells (**Fig. 4a**–**e**). To determine whether UTX was physically recruited to those promoters, we analyzed UTX in sorted control *i*NKT cells by ChIP followed by PCR (ChIP-PCR). We detected significantly greater occupancy of UTX at the promoter regions of the representative genes *Tbx21*, *Il2rb*, *S100a6* and *Klrd1* relative to its occupancy at the housekeeping (control) gene encoding β-actin (*Actb*), which was not regulated by UTX, on the basis of gene expression and ChIP-Seq data (**Fig. 4f**). These results suggested that UTX directly controlled the epigenetic

landscape around the promoters of *i*NKT cell lineage-specific genes to facilitate their transcription.

### Requirement for UTX enzyme activity in *i*NKT cell development

Although the data above indicated a critical role for UTX in regulating *i*NKT-cell-lineage-specific gene expression and development, it was important to assess whether UTX acted directly in *i*NKT cells. A 'peculiarity' of *i*NKT cells is that they originate from and concomitantly are selected by DP thymocytes[38]. This feature allows the use of mixed-bone-marrow chimera to distinguish whether a gene defect is intrinsic to *i*NKT cells or if extrinsic antigen presentation and selection by CD1d-expressing DP thymocytes is responsible for an observed phenotype. We transferred bone marrow cells from control and UTX-deficient mice (at a 1:1 ratio) into immunodeficient *Rag2*^−/− host mice and subsequently determined the contribution of each genotype of donor bone marrow to the overall *i*NKT cell pool in the recipients. In the thymus, the population of stage 0–1 *i*NKT cells of UTX-deficient origin predominated over that of control cells (**Supplementary Fig. 7a,b**), due to the relative accumulation of immature *i*NKT cells in UTX deficiency. Accordingly, the majority of *i*NKT cells at stage 3 were of control origin (**Supplementary Fig. 7a,b**), again indicative of a block of maturation in the absence of UTX. In the liver, most *i*NKT cells were control cells, and few UTX-deficient cells contributed to the peripheral *i*NKT cell pool (**Supplementary Fig. 7c**). Conventional T cells displayed a balanced mixed chimerism (**Supplementary Fig. 7c**), which highlighted a specific effect of UTX on *i*NKT cells. Thus, the block in maturation reflected an intrinsic defect in *i*NKT cells imposed by loss of UTX that was not 'rescued' by the presence of control DP thymocytes.

Next we sought to determine whether the downregulated gene-expression program and developmental block of *i*NKT cells could be 'rescued' by *in vivo* reconstitution with UTX and whether its demethylase activity was required for this. To investigate this, we used lentiviral transduction of bone marrow cells, followed by transplantation of the cells into *Rag2*^−/− host mice. UTX-deficient bone marrow
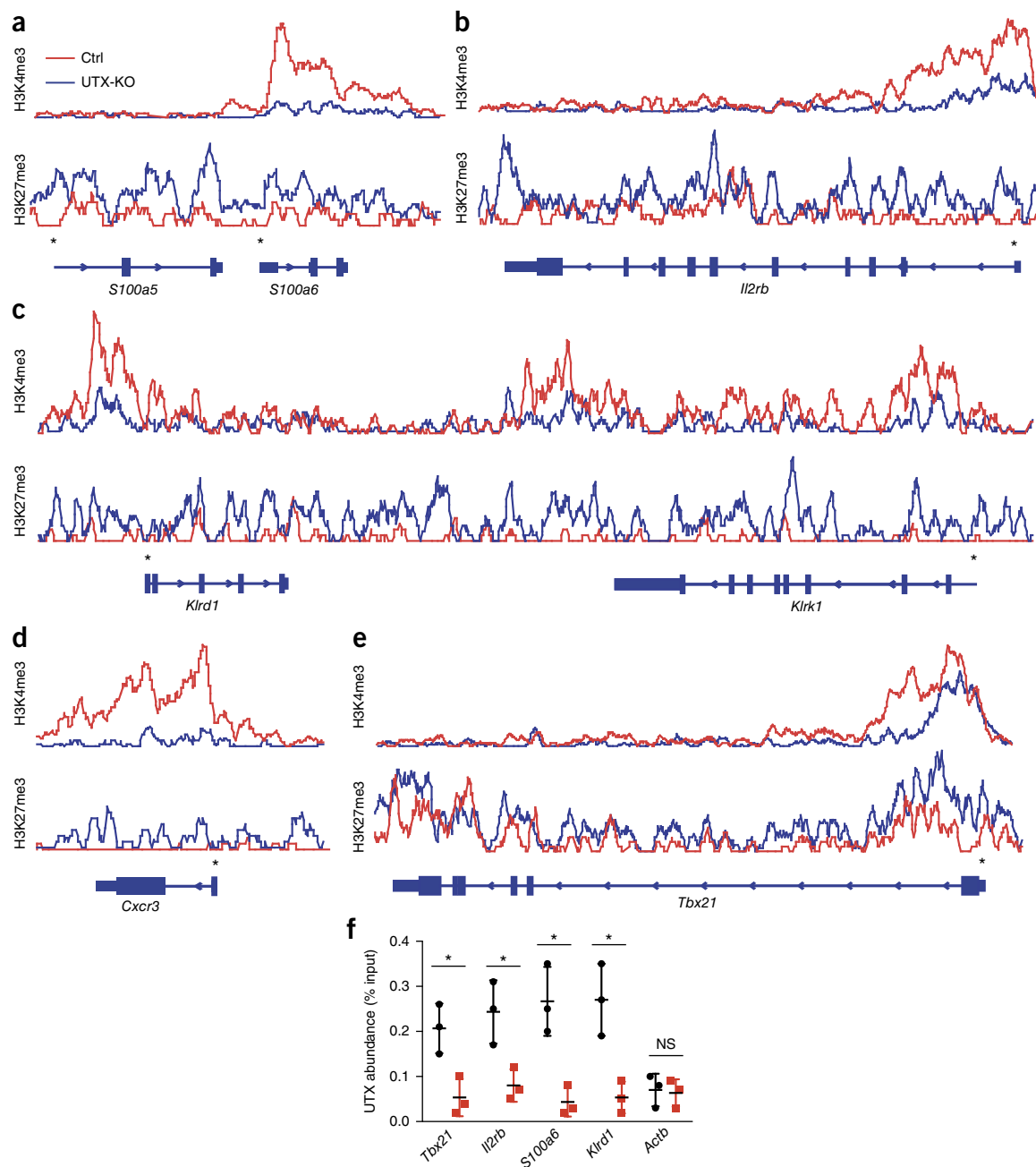
**Figure 4** UTX occupies the promoters of *i*NKT cell signature genes that exhibit UTX-dependent chromatin regulation. (**a**–**e**) ChIP-Seq overlay tracks of H3K27me3 and H3K4me3 marks for the *i*NKT cell signature genes *S100a5* and *S100a6* (**a**), *Il2rb* (**b**), *Klrd1* and *Klrk1* (**c**), *Cxcr3* (**d**) and *Tbx21* (**e**) in UTX-sufficient (control) and UTX-KO *i*NKT cells (key) (data from **Fig. 3**); below plots, gene structure and direction of transcription (*, promoter). (**f**) ChIP-PCR analysis of UTX occupancy around the promoters of signature genes as in **a**–**e** and *Actb* (negative control), presented as enrichment for promoter sequences relative to that obtained by ChIP with isotype-matched control antibody (IgG). *$P < 0.05$ (unpaired *t*-test). Data are from three independent experiments (mean ± s.d. in **f**).

transduced with empty virus failed to produce a substantial population of *i*NKT cells in the thymus (**Fig. 5a**). Notably, UTX-KO bone marrow reconstituted with full-length UTX exhibited substantial *i*NKT cell development, whereas reconstitution with mutant UTX lacking enzymatic activity failed to generate a sizeable *i*NKT cell population (**Fig. 5a**). Upon analysis of the various maturation stages of *i*NKT cells, we observed that the few UTX-KO *i*NKT cells that developed from bone marrow transduced with empty virus or virus encoding mutant UTX lacking enzymatic activity were unable to fully mature

to stage 3 (**Fig. 5b**). In contrast, reconstitution with full-length UTX facilitated the complete development of *i*NKT cells in the thymus (**Fig. 5b**). We found that liver *i*NKT cells were almost completely absent from the UTX-KO mice transduced with empty virus (**Fig. 5c,d**). Reconstitution with full-length UTX 'rescued' this phenotype via the generation of a sizeable liver *i*NKT cell population, whereas only a very minor *i*NKT cell fraction developed in the presence of mutant UTX lacking enzymatic activity (**Fig. 5c,d**). We demonstrated that expression of the gene encoding UTX was similar in mice reconstituted
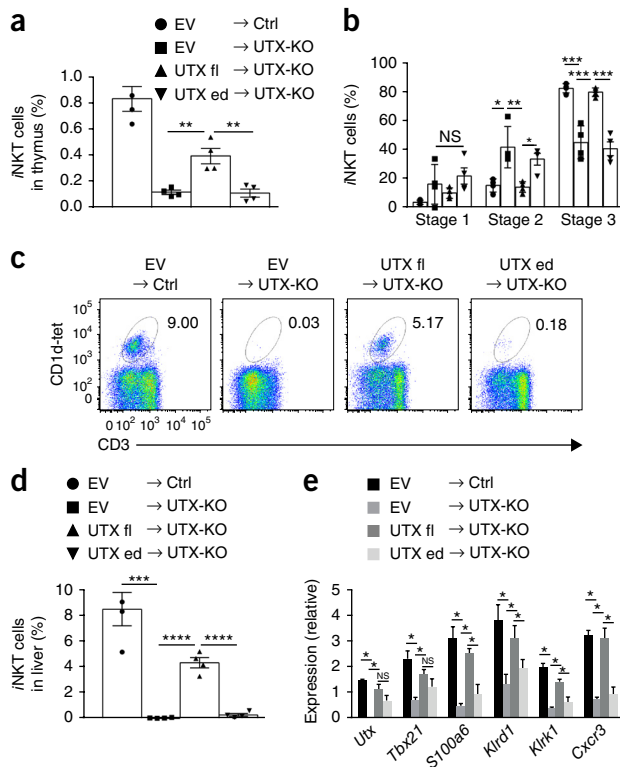
**Figure 5** The demethylase activity of UTX is required for the generation of *i*NKT cells. (**a**) Frequency of thymic *i*NKT cells in *Rag2*$^{-/-}$ host mice 12 weeks after transfer of UTX-sufficient (control) bone marrow cells transduced (→) with lentivirus containing empty vector (EV) or UTX-KO bone marrow cells transduced with lentivirus containing empty vector or vector encoding full-length UTX (UTX fl) or UTX lacking enzymatic activity (UTX ed), assessed by flow cytometry. (**b**) Frequency of thymic *i*NKT cells from mice as in **a** (key) in stages 1–3 (horizontal axis; as in **Fig. 1b,c**). (**c**) Flow cytometry of liver *i*NKT cells from mice as in **a**. Numbers adjacent to outlined areas indicate percent CD1d-tet$^+$CD3$^+$ cells. (**d**) Frequency of liver *i*NKT cells as in **c**. (**e**) Quantitative RT-PCR analysis of *Utx* and signature genes (horizontal axis) in thymic *i*NKT cells from mice as in **a**; results were normalized to those of *Actb*. Each symbol (**a**,**b**,**d**) represents an individual mouse. NS, not significant ($P > 0.05$); *$P < 0.05$, **$P < 0.01$, ***$P < 0.001$ and ****$P < 0.0001$ (one-way ANOVA and multiple comparisons). Data are from two independent experiments with four mice per group (mean ± s.e.m. in **a**,**b**,**d**,**e**).

with full-length UTX and those reconstituted with mutant UTX lacking enzymatic activity (**Fig. 5e**), which indicated no difference in reconstitution efficiency. In parallel, we analyzed the expression of signature genes in *i*NKT cells from the thymus of reconstituted mice. Notably, reconstitution with full-length UTX restored expression of the *i*NKT cell gene signature, including *Tbx21*, *Klrd1* and *Cxcr3* (**Fig. 5e**). In contrast, mutant UTX lacking enzymatic activity failed to restore signature-gene expression, although an enzyme-independent contribution was observed for *Tbx21* (**Fig. 5e**). Together these data demonstrated that the enzymatic demethylase function of UTX was essential for the proper generation of *i*NKT cells by establishing the *i*NKT cell gene-expression program.

### Regulation of *i*NKT cell development by JunB

To gain further mechanistic insights how UTX regulates gene expression in *i*NKT cells, we performed motif-enrichment analysis (using the analysis tool Haystack) and identified potential transcription factors that might work together with UTX on the promoters of *i*NKT cell

signature genes. We found significant enrichment for target motifs for the AP-1 transcription factors JunB and JunD in cluster 3, as well as those for the transcription factor RAR-RXR in cluster 4, around the promoters of genes that showed UTX-dependent chromatin and transcriptional regulation (**Fig. 6a**). To determine whether JunB directly regulates UTX-dependent *i*NKT cell genes, we performed ChIP-PCR analysis of JunB. JunB bound to the promoters of signature genes from cluster 3 that showed enrichment for JunB motifs (*Il2rb* and *Klrd1*) (**Fig. 6b** and **Supplementary Table 2**). To determine whether UTX acted together with this putative *i*NKT cell transcription factor, we immunoprecipitated proteins from lysates of *i*NKT cells and demonstrated that UTX interacted with JunB (**Fig. 6c**). Notably, UTX was also able to specifically bind to the *i*NKT cell transcription factor PLZF (**Fig. 6c**). Furthermore, JunB expression was induced 'preferentially' in *i*NKT cells relative to its expression in other thymocyte subsets (**Fig. 6d**), indicative of a potential role for JunB in the generation of *i*NKT cells. To test that hypothesis, we analyzed JunB-deficient (JunB-KO) mice and found that the frequency of conventional CD4$^+$ T cells and CD8$^+$ T cells, as well as that of CD4$^-$CD8$^-$ (double-negative) and DP thymocytes, was similar in JunB-KO mice and JunB-sufficient (control) mice (**Fig. 6e**). However, the frequency of thymic and peripheral *i*NKT cells was significantly lower in JunB-KO mice than in control mice (**Fig. 6f,g**). To investigate whether JunB regulated the transcription of *i*NKT cell signature genes with UTX-dependent transcriptional and chromatin regulation in cluster 3, we performed quantitative PCR analysis of sorted thymic *i*NKT cells from control and JunB-KO mice. We found that the signature genes *Il2rb* and *Klrd1* (whose promoters were both bound by JunB; **Fig. 6b**) were significantly downregulated in JunB-KO *i*NKT cells relative to their expression in control *i*NKT cells (**Fig. 6h**). Together these results showed that UTX interacted with transcription factors such as JunB to establish lineage-specific gene expression in *i*NKT cells.

### UTX-deficient *i*NKT cells fail to activate PLZF target genes

Given the finding of a physical association of UTX with PLZF, we sought to determine whether UTX regulated the PLZF-mediated activation of gene expression in *i*NKT cells. Through the use of a PLZF ChIP-Seq data set that defined PLZF-activated genes in *i*NKT cells[39], we determined that loss of UTX in *i*NKT cells led to impaired activation of the expression of PLZF target genes (**Fig. 7a**). PLZF-activated target genes were significantly downregulated in UTX-KO *i*NKT cells relative to the expression of randomly selected (control) genes (**Fig. 7b**). To assess whether that downregulation was accompanied by accumulation of H3K27me3 at the promoter of those genes in UTX-KO *i*NKT cells, we compared the average abundance of H3K27me3 around the promoters of PLZF-activated target genes and those of randomly selected (control) genes. We found that the abundance of H3K27me3 around the promoters of PLZF-activated genes was significantly greater in UTX-KO *i*NKT cells than in control cells, but its abundance around the 'random' (control) genes was not (**Fig. 7c**). Overlay tracks for PLZF target genes, including *Il18r1*, *Il12rb1* and *Eya2*, demonstrated distinct UTX-dependent accumulation of H3K27me3 and a concomitant decrease in H3K4me3 around the promoter regions that PLZF occupied (**Fig. 7d–f**). Accordingly, we confirmed that the expression of *Il18r1*, *Il12rb1* and *Eya2* was significantly lower in UTX-KO *i*NKT cells than in control cells (**Fig. 7g**). These data indicated that UTX controlled the epigenetic landscape and transcription of PLZF-activated genes.

### UTX facilitates accessibility of *i*NKT cell super-enhancers

Because super-enhancers bestow lineage specificity[14,15] and *i*NKT cells are vulnerable to the effects of the loss of UTX, we hypothesized

that another mechanism by which UTX controls commitment to the *i*NKT cell lineage might be through regulation of super-enhancer accessibility. First, we delineated the super-enhancer landscape of *i*NKT cells by genome-wide ChIP-Seq analysis of histone H3 acetylated at Lys27 (H3K27ac) and defined super-enhancers as large enhancer elements with a substantial abundance of H3K27ac[14,15]. We identified 396 super-enhancers that included elements proximal to genes encoding known regulators of the *i*NKT cell lineage, such as *Tbx21*, *Zbtb16* and *Il2rb*, as well as those encoding regulators not previously characterized in *i*NKT cells, including the transcription factor JunB (**Fig. 8a**,**b**, **Supplementary Fig. 8a**,**b** and **Supplementary Table 3**). To reveal potential pathways associated with genes proximal to the super-enhancers identified in *i*NKT cells, we performed GREAT analysis of the super-enhancer elements. We found significant enrichment for the AP-1 pathway in our analysis (**Supplementary Fig. 8c**), which confirmed the identification of JunB as a crucial, previously unknown regulator of the *i*NKT cell lineage.

To determine whether the accessibility of super-enhancers in *i*NKT cells was affected by the absence of UTX, we performed ATAC-Seq ('assay

for transposase-accessible chromatin using sequencing')[40] that captured accessible chromatin regions in sorted control and UTX-KO *i*NKT cells. Among the 396 super-enhancers we identified, 109 super-enhancers had control-cell-specific ATAC-Seq peaks and therefore lost accessibility in UTX-KO *i*NKT cells (**Fig. 8c** and **Supplementary Table 4**). By comparing the ratio of gene expression (log$_2$ values) in control cells to that in UTX-KO cells for these genes to that ratio for all genes, we found that genes near super-enhancers that showed UTX-dependent accessibility were downregulated in UTX-KO *i*NKT cells (**Fig. 8d**).

To determine whether that loss of accessibility of super-enhancers and diminished transcription of nearby genes was accompanied by accumulation of H3K27me3 in UTX deficiency, we compared average abundance of H3K27me3 around the defined *i*NKT cell super-enhancer regions with that of randomly selected control regions in UTX-KO *i*NKT cells. We detected significant accumulation of H3K27me3 around super-enhancer regions in UTX-KO *i*NKT cells (**Fig. 8e**). In control *i*NKT cells, super-enhancer regions exhibited a lower abundance of H3K27me3 than that of randomly selected (control) regions (**Fig. 8e**), consistent with the conclusion that active enhancers are
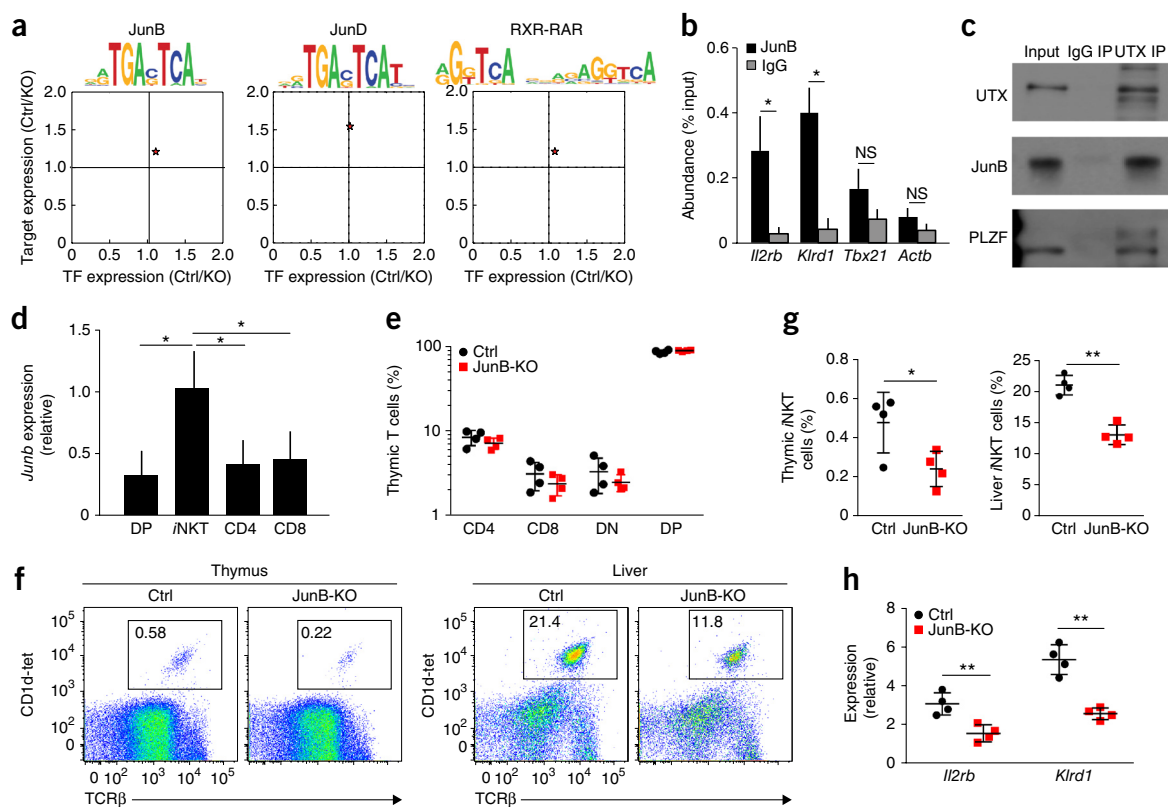


**Figure 6** JunB partners with UTX to regulate the *i*NKT cell signature and development. (**a**) Expression of the AP-1 transcription factors (TF) JunB (left), JunD (middle) and RXR-RAR (right) plotted against that of their targets (vertical axes), all presented as a ratio of expression in UTX-sufficient cells to that in UTX-KO cells (Ctrl/KO); above plots, target motif sequence. For motif enrichment, the analysis tool Haystack was used: $P = 0.006$ (JunB and JunD) or 0.005 (RXR-RAR). The large asterisks indicate the values of the ratios in the plots. (**b**) ChIP-PCR analysis of JunB or IgG (key) at the promoters of UTX-dependent genes (horizontal axis) and *Actb* (negative control) in thymic *i*NKT cells (presented as in **Fig. 4f**). (**c**) Immunoprecipitation (IP) and immunoblot analysis of the molecular interaction among UTX, JunB and PLZF in *i*NKT cells (far left, 10% input; middle, immunoprecipitation with an isotype-matched control antibody (IgG)). (**d**) Quantitative RT-PCR analysis of the gene encoding JunB (*Junb*) in thymic DP cells (DP), *i*NKT cells (*i*NKT), CD4+ cells (CD4) and CD8+ cells (CD8); results were normalized to those of *Actb*. (**e**) Frequency of thymic CD4+, CD8+, CD4−CD8− double-negative (DN) and DP T cells in JunB-sufficient (control (Ctrl)) and JunB-KO mice (key). (**f**) Flow cytometry of thymic and liver *i*NKT cells in control and JunB-KO mice. Numbers in outlined areas indicate percent CD1d-tet+TCRβ+ cells. (**g**) Frequency of thymic and liver *i*NKT cells as in **f**. (**h**) Quantitative RT-PCR analysis of the UTX-dependent *i*NKT cell signature genes *Il12rb* and *Klrd1* in control and JunB-KO thymic *i*NKT cells (key); results were normalized to those of *Actb*. Each symbol (**e**,**g**,**h**) represents an individual mouse; small horizontal lines indicate the mean (± s.e.m.). *$P < 0.05$ and **$P < 0.01$ (unpaired *t*-test). Data are representative of two independent experiments (**a**) or three independent experiments (**c**) or are from three independent experiments (**b**,**d**; mean + s.d.) or two experiments with four mice per group (**e**–**h**).
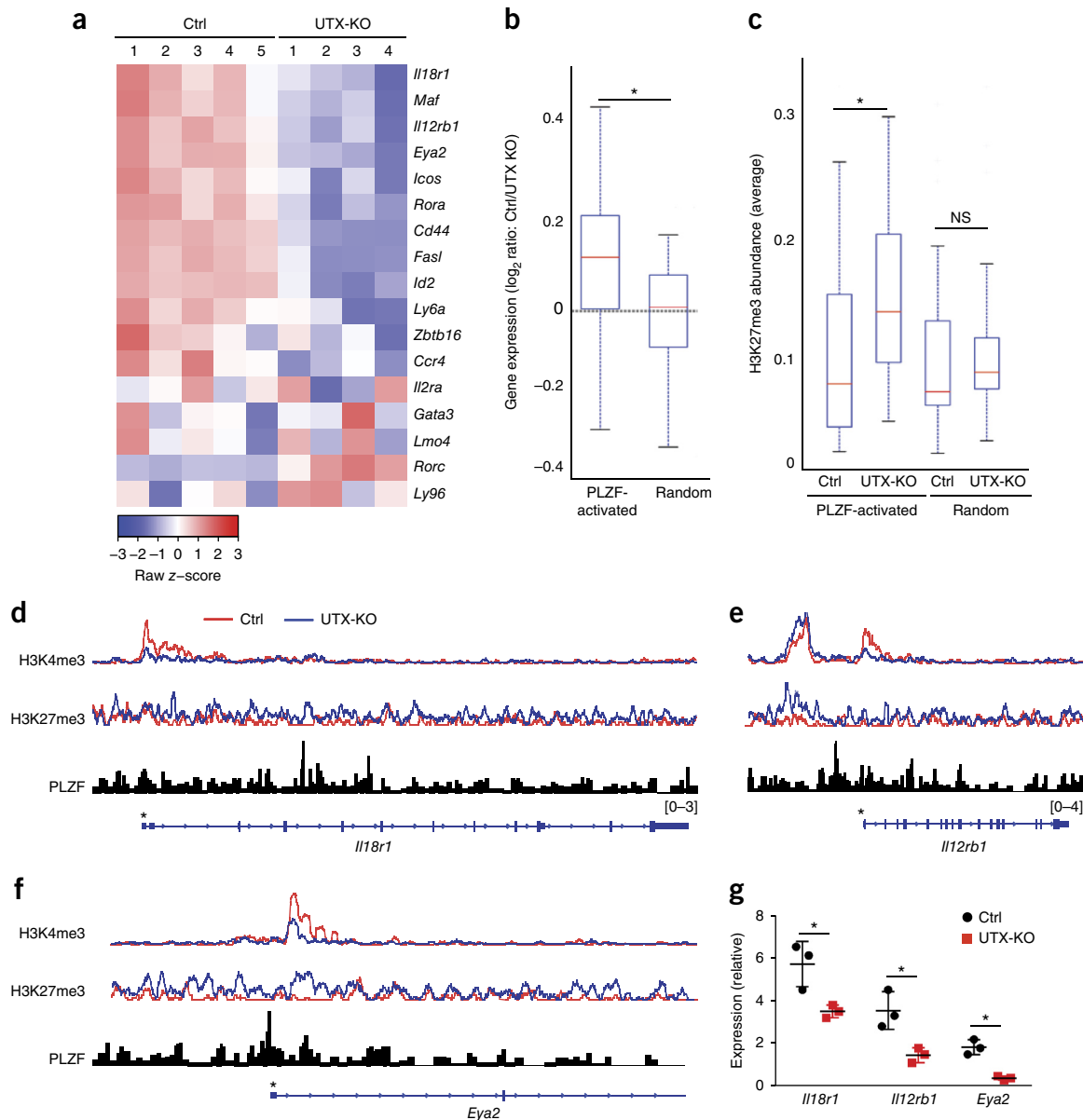
**Figure 7** UTX deficiency impairs the activation of PLZF target genes in *i*NKT cells. (**a**) Expression of PLZF-activated genes (right margin) in UTX-sufficient (control (Ctrl)) and UTX-KO *i*NKT cells, presented as *z*-scores (key); numbers above the columns indicate biological replicates. (**b**) Expression of PLZF-activated genes and 'random' (control) genes (horizontal axis), presented as the log$_2$ ratio of expression in control cells to that in UTX-KO cells (Ctrl/UTX-KO) (boxes extend from the lower to upper quartile values; small horizontal line indicates the median (whiskers, 1.5 inter-quartile range)). (**c**) Abundance of H3K27me3 marks (average values) around the promoters (within 1 kb (upstream or downstream) of the TSS) of PLZF-activated genes and 'random' (control) genes ($n = 17$ regions per group) in control and UTX-KO *i*NKT cells (boxes extend from the lower to upper quartile values; small horizontal line indicates the median (whiskers, 1.5 inter-quartile range)). (**d–f**) Abundance of H3K4me3 and H3K27me3 around the PLZF-activated genes *Il18r1* (**d**), *Il12rb1* (**e**) and *Eya2* (**f**); below, gene structure (as in **Fig. 4a–e**). (**g**) Quantitative RT-PCR analysis of the PLZF-activated genes *Il18r1*, *Il12rb1* and *Eya2* in control and UTX-KO thymic *i*NKT cells; results were normalized to those of *Actb*. Each symbol represents an individual mouse; small horizontal lines indicate the mean (± s.e.m.). *$P < 0.05$ (Mann-Whitney *U* test (**b**,**c**) or unpaired *t*-test (**g**)). Data are from two independent experiments (**a–f**) or three independent experiments (**g**).

devoid of H3K27me3 (refs. 17,41). The randomly selected (control) regions in control *i*NKT cells and those in UTX-KO *i*NKT cells had a similar abundance of H3K27me3 (**Fig. 8e**). Notably, super-enhancers that showed UTX-dependent accessibility were near genes encoding important regulators of *i*NKT cells, such as *Tbx21* (**Fig. 8f** and **Supplementary Fig. 8a**) and *Il2rb* (**Fig. 8g** and **Supplementary Fig. 8b**). Furthermore, GREAT analysis demonstrated enrichment, around these regions, for genes encoding products involved in lymphocyte differentiation and IL-2 signaling (**Supplementary Fig. 8d**). To deter-

mine the transcription factors that bind these super-enhancers, we performed motif analysis and found enrichment for the transcription factors RelA and Bhlhe40 (**Supplementary Fig. 8e**). Bhlhe40 has been shown to act together with T-bet to control *i*NKT cell function[42]. Although a small fraction of super-enhancers (13) gained accessibility in UTX-KO *i*NKT cells (**Fig. 8c** and **Supplementary Table 4**), we did not detect any gene-set enrichment for these regions (**Supplementary Fig. 8d**). Overall, these results suggested that UTX regulated the accessibility of super-enhancers that establish *i*NKT cell identity.
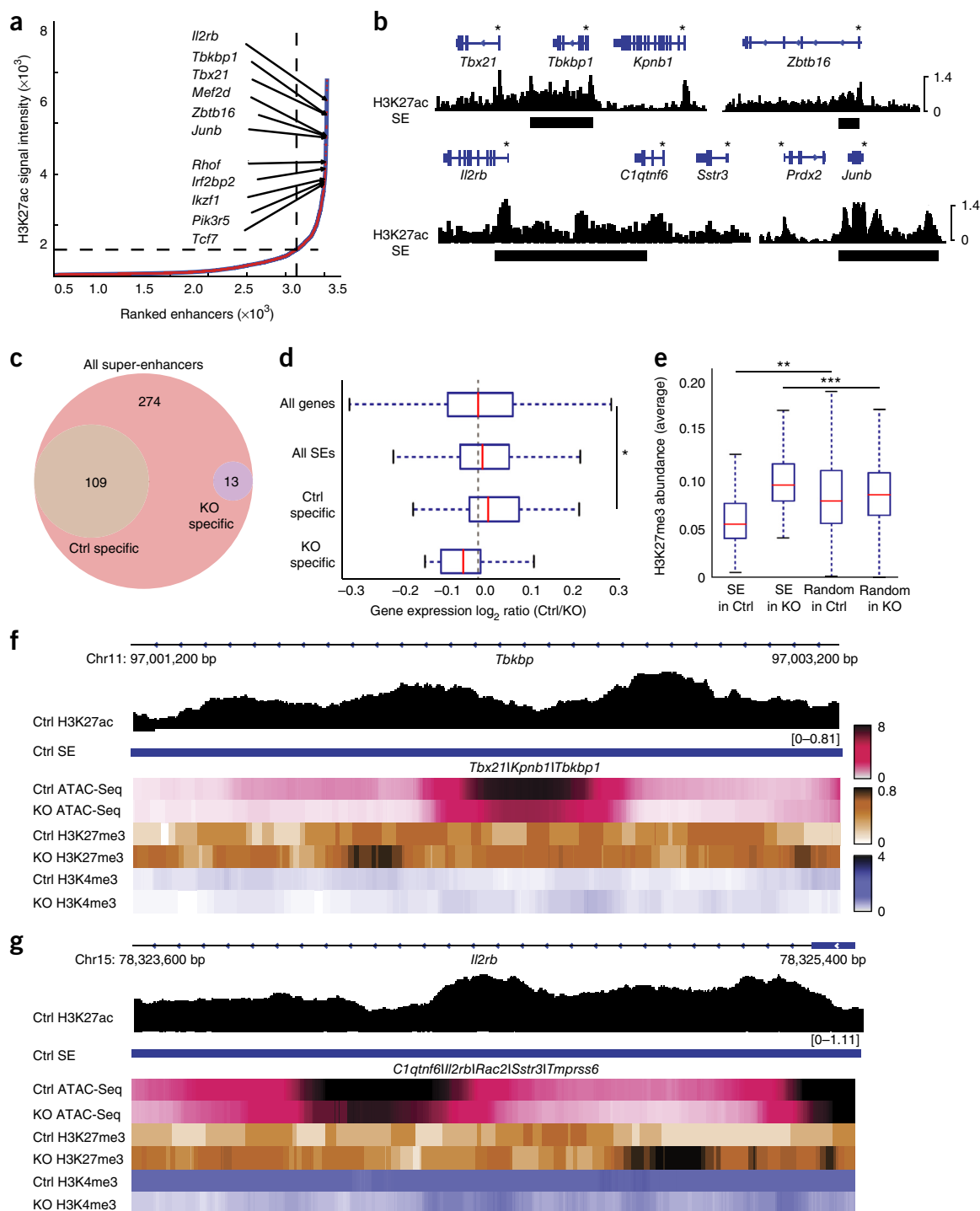
**Figure 8** UTX facilitates the accessibility of super-enhancers in *i*NKT cells. (**a**) Ranking of super-enhancers in *i*NKT cells on the basis of the signal intensity of H3K27ac (ROSE algorithm). (**b**) ChIP-Seq analysis of H3K27ac in the super-enhancers of various genes in *i*NKT cell; above plots, gene bodies (black bars, super-enhancers; *, promoter). (**c**) ATAC-Seq of chromatin accessibility of the super-enhancers in **a**, showing all super-enhancers (full circle) and those with specific peaks in control *i*NKT cells (bottom left) or UTX-KO *i*NKT cells (bottom right). (**d**) Expression of all genes (top; $n = 20,628$), genes near all defined *i*NKT cell super-enhancers (All SEs; $n = 396$) or *i*NKT cell super-enhancers with accessibility specific to control cells (Ctrl specific; $n = 109$) or UTX-KO cells (KO specific; $n = 13$), presented as the ratio of expression ($\log_2$ values) in control cells to that in UTX-KO cells (Ctrl/KO) (boxes extend from the lower to upper quartile values; small horizontal line indicates the median (whiskers, 1.5 inter-quartile range)). (**e**) Abundance of H3K27me3 marks (average values) around the super-enhancer regions in **a** and randomly selected control regions (Random) in control and UTX-KO *i*NKT cells ($n = 396$ regions per group) (boxes extend from the lower to upper quartile values; small horizontal line indicates the median (whiskers, 1.5 inter-quartile range)). (**f**,**g**) ChIP-Seq analysis of H3K27ac (top), super-enhancers defined (by the ROSE algorithm) in control cells (Ctrl SE), ATAC-Seq analysis of control and UTX-KO *i*NKT cells (third and fourth rows), and analysis of the distribution of H3K27me3 and H3K4me3 (below) in control and UTX-KO *i*NKT cells, around the defined super-enhancer regions for *Tbx21* (which encodes T-bet) (**f**) and *Il2rb* (**g**). $P = 0.14$ (control regions, **e**); *$P = 0.002$, **$P = 5.9 \times 10^{-10}$ and ***$P = 1.9 \times 10^{-14}$ (Mann-Whitney $U$-test). Data are from two independent experiments.

## DISCUSSION

Discoveries of key transcription factors[8,9,11] and gene-expression programs[13] have contributed to the understanding of the *i*NKT cell lineage. In this context, a published study has demonstrated the diversity of gene programs in different *i*NKT cell subsets on the basis of RNA-sequencing transcriptomics and the description of enhancer elements[43]. However, the epigenetic mechanisms that govern *i*NKT cell identity have remained undefined. Here we demonstrated a selective, cell-intrinsic and catalytic role for the H3K27me3 demethylase UTX in regulating the epigenetic landscape and lineage-specific gene expression of *i*NKT cells. Our data and a published study[35] have revealed a requirement for the H3K27me3 demethylases UTX and JMJD3 in the development of *i*NKT cells. We found that this requirement was due to UTX-dependent regulation of the expression of *i*NKT cell signature genes. UTX-deficient *i*NKT cells exhibited a developmental block and failed to induce the expression of genes encoding transcription factors and signaling molecules involved in the terminal maturation of *i*NKT cells, such as T-bet (*Tbx21*)[11] and CD122 (*Il2rb*)[9,10].

Epigenetic regulation of gene expression by UTX has been studied mainly in the context of the demethylation of repressive H3K27me3 marks. Moreover, UTX associates with MLL2, which catalyzes trimethylation of H3K4 at promoters to facilitate the transcription of genes encoding lineage-specifying factors[21,23,29]. Accordingly, in *i*NKT cells, the promoters of UTX-dependent signature genes, such as those in *Tbx21* and *Il2rb*, accumulated H3K27me3 and harbored a lower abundance of H3K4me3 in the absence of UTX.

We found that gene promoters that exhibited UTX-dependent chromatin and transcriptional regulation were bound by the AP-1 transcription factor JunB. A published report showing that JunB is part of a gene network 'preferentially' upregulated in *i*NKT cells relative to their expression in NK cells and conventional T cells[13] is consistent with our findings. While indirect evidence, through overexpression or deficiency of the negative regulator BATF, has shown that AP-1 activity promotes generation of *i*NKT cells[44,45], lack of the AP-1 family member Fra2 leads to an increased number of *i*NKT cells[46]. Interestingly, JunB–AP-1 directly controls expression of the gene encoding IFN-γ, a hallmark cytokine released by mature *i*NKT cells[47]. Our studies revealed significantly fewer thymic as well as peripheral *i*NKT cells in JunB-deficient mice than in JunB-sufficient mice. Together our data have identified JunB as a previously unknown regulator that influences *i*NKT cell development.

UTX can function in a way that is both dependent on and independent of its demethylase enzyme activity[29,48]. We found that the development of *i*NKT cells required the demethylase activity of UTX, indicative of a critical role for the removal of H3K27me3 marks from the promoters of *i*NKT cell signature genes. Interestingly, *i*NKT cells lacking components of PRC2, which is responsible for the deposition of H3K27me3, exhibit impaired maturation and increased accumulation in the thymus and spleen[35,49]. It has been proposed that the development of *i*NKT cells involves a transition in the promoter of *Zbtb16* (which encodes PLZF) from a poised state in DP thymocytes, harboring both H3K27me3 marks and H3K4me3 marks, to an active state in *i*NKT cells, characterized by H3K4me3 and a lack of H3K27me3 (ref. 35). Although we did not observe substantial accumulation of H3K27me3 around the promoter of *Zbtb16* or a robust decrease in PLZF expression in UTX-deficient *i*NKT cells, we demonstrated that UTX regulated the expression and epigenetic landscape of PLZF-activated genes in *i*NKT cells.

Published studies have identified super-enhancers on the basis of elevated abundance of H3K27ac as a hallmark of key genes associated with cell identity and genetic risk of disease[14,15,50]. Our study has defined the *i*NKT cell super-enhancer landscape and has demonstrated that signature genes, including *Zbtb16*, *Tbx21* and *Il2rb*, exhibited super-enhancer elements. In addition, we identified numerous previously unknown regulators of *i*NKT cell identity, which should provide an invaluable resource for understanding the epigenetic control of specification to the *i*NKT cell lineage and disease-associated genes in *i*NKT cells.

UTX interacts with chromatin regulators such as SWI/SNF and the MLL complex that can affect enhancer activation[23,29,48]. Since dynamic regulation of the abundance of H3K27me3 and H3K27ac determines enhancer activity[17,41], another mechanism for UTX-mediated gene regulation raised by our study involved the control of the accessibility of lineage-specific super-enhancers by UTX in *i*NKT cells. The accessibility of super-enhancers near downregulated signature genes, such as *Tbx21* and *Il2rb*, was lost in UTX-deficient *i*NKT cells. That finding suggested that the proper maturation of *i*NKT cells requires a dual mechanism that involves UTX-mediated regulation of the epigenetic landscape around both the promoters of signature genes and their enhancers. Collectively, our data offer a new perspective on the transcriptional control of *i*NKT cell development and delineate multiple mechanisms that UTX engages to regulate the lineage-specific gene-expression program of *i*NKT cells.

## METHODS

Methods, including statements of data availability and any associated accession codes and references, are available in the online version of the paper.

*Note: Any Supplementary Information and Source Data files are available in the online version of the paper.*

### AUTHOR CONTRIBUTIONS

S.B. designed, performed and interpreted experiments involving gene expression analysis, ChIP-Seq, ATAC-Seq, lentiviral transduction, qRT-PCR, ChIP-PCR and immunoprecipitation, with help from M.E.X., and generated UTX-KO and JMJD3-KO mice, with help from M.A.K.; J.H.K. designed, performed and interpreted experiments involving *i*NKT cell analysis by flow cytometry with help from Y.H.; L.P. designed, performed and interpreted bioinformatics analysis with help from J.H.; P.P.D., R.A.B. and R.D. assisted with ChIP-Seq analysis; A.H. and E.P. provided JunB-KO mice; W.N.H. and Ö.H.Y. participated in the design and interpretation of experiments; G.-C.Y. supervised bioinformatics analysis; S.H.O. and F.W. designed and supervised experiments; and S.B., J.H.K., S.H.O. and F.W. wrote the manuscript with support from L.P.

### COMPETING FINANCIAL INTERESTS

The authors declare no competing financial interests.

Reprints and permissions information is available online at http://www.nature.com/reprints/index.html.

1. Bendelac, A., Savage, P.B. & Teyton, L. The biology of NKT cells. *Annu. Rev. Immunol.* **25**, 297–336 (2007).
2. Rossjohn, J., Pellicci, D.G., Patel, O., Gapin, L. & Godfrey, D.I. Recognition of CD1d-restricted antigens by natural killer T cells. *Nat. Rev. Immunol.* **12**, 845–857 (2012).

3. Kawano, T. *et al.* CD1d-restricted and TCR-mediated activation of Vα14 NKT cells by glycosylceramides. *Science* **278**, 1626–1629 (1997).

4. Cui, J. *et al.* Requirement for Vα14 NKT cells in IL-12-mediated rejection of tumors. *Science* **278**, 1623–1626 (1997).

5. Bendelac, A. Positive selection of mouse NK1+ T cells by CD1-expressing cortical thymocytes. *J. Exp. Med.* **182**, 2091–2096 (1995).

6. Lazarevic, V. *et al.* The gene encoding early growth response 2, a target of the transcription factor NFAT, is required for the development and maturation of natural killer T cells. *Nat. Immunol.* **10**, 306–313 (2009).

7. Kovalovsky, D. *et al.* The BTB-zinc finger transcriptional regulator PLZF controls the development of invariant natural killer T cell effector functions. *Nat. Immunol.* **9**, 1055–1064 (2008).

8. Savage, A.K. *et al.* The transcription factor PLZF directs the effector program of the NKT cell lineage. *Immunity* **29**, 391–403 (2008).

9. Seiler, M.P. *et al.* Elevated and sustained expression of the transcription factors Egr1 and Egr2 controls NKT cell lineage differentiation in response to TCR signaling. *Nat. Immunol.* **13**, 264–271 (2012).

10. Matsuda, J.L. *et al.* Homeostasis of Vα14i NKT cells. *Nat. Immunol.* **3**, 966–974 (2002).

11. Townsend, M.J. *et al.* T-bet regulates the terminal maturation and homeostasis of NK and Vα14i NKT cells. *Immunity* **20**, 477–494 (2004).

12. Engel, I. & Kronenberg, M. Transcriptional control of the development and function of Vα14i NKT cells. *Curr. Top. Microbiol. Immunol.* **381**, 51–81 (2014).

13. Cohen, N.R. *et al.* Shared and distinct transcriptional programs underlie the hybrid nature of iNKT cells. *Nat. Immunol.* **14**, 90–99 (2013).

14. Whyte, W.A. *et al.* Master transcription factors and mediator establish super-enhancers at key cell identity genes. *Cell* **153**, 307–319 (2013).

15. Hnisz, D. *et al.* Super-enhancers in the control of cell identity and disease. *Cell* **155**, 934–947 (2013).

16. Kouzarides, T. Chromatin modifications and their function. *Cell* **128**, 693–705 (2007).

17. Rada-Iglesias, A. *et al.* A unique chromatin signature uncovers early developmental enhancers in humans. *Nature* **470**, 279–283 (2011).

18. Creyghton, M.P. *et al.* Histone H3K27ac separates active from poised enhancers and predicts developmental state. *Proc. Natl. Acad. Sci. USA* **107**, 21931–21936 (2010).

19. Simon, J.A. & Kingston, R.E. Mechanisms of polycomb gene silencing: knowns and unknowns. *Nat. Rev. Mol. Cell Biol.* **10**, 697–708 (2009).

20. Bernstein, B.E. *et al.* A bivalent chromatin structure marks key developmental genes in embryonic stem cells. *Cell* **125**, 315–326 (2006).

21. Agger, K. *et al.* UTX and JMJD3 are histone H3K27 demethylases involved in HOX gene regulation and development. *Nature* **449**, 731–734 (2007).

22. Lan, F. *et al.* A histone H3 lysine 27 demethylase regulates animal posterior development. *Nature* **449**, 689–694 (2007).

23. Lee, M.G. *et al.* Demethylation of H3K27 regulates polycomb recruitment and H2A ubiquitination. *Science* **318**, 447–450 (2007).

24. De Santa, F. *et al.* The histone H3 lysine-27 demethylase Jmjd3 links inflammation to inhibition of polycomb-mediated gene silencing. *Cell* **130**, 1083–1094 (2007).

25. Heintzman, N.D. *et al.* Histone modifications at human enhancers reflect global cell-type-specific gene expression. *Nature* **459**, 108–112 (2009).

26. Welstead, G.G. *et al.* X-linked H3K27me3 demethylase Utx is required for embryonic development in a sex-specific manner. *Proc. Natl. Acad. Sci. USA* **109**, 13004–13009 (2012).

27. Mansour, A.A. *et al.* The H3K27 demethylase Utx regulates somatic and germ cell epigenetic reprogramming. *Nature* **488**, 409–413 (2012).

28. Li, Q. *et al.* Critical role of histone demethylase Jmjd3 in the regulation of CD4+ T-cell differentiation. *Nat. Commun.* **5**, 5780 (2014).

29. Lee, S., Lee, J.W. & Lee, S.K. UTX, a histone H3-lysine 27 demethylase, acts as a critical switch to activate the cardiac developmental program. *Dev. Cell* **22**, 25–37 (2012).

30. Thieme, S. *et al.* The histone demethylase UTX regulates stem cell migration and hematopoiesis. *Blood* **121**, 2462–2473 (2013).

31. Ntziachristos, P. *et al.* Contrasting roles of histone 3 lysine 27 demethylases in acute lymphoblastic leukaemia. *Nature* **514**, 513–517 (2014).

32. van Haaften, G. *et al.* Somatic mutations of the histone H3K27 demethylase gene UTX in human cancer. *Nat. Genet.* **41**, 521–523 (2009).

33. Cook, K.D. *et al.* T follicular helper cell-dependent clearance of a persistent virus infection requires T cell expression of the histone demethylase UTX. *Immunity* **43**, 703–714 (2015).

34. Manna, S. *et al.* Histone H3 lysine 27 demethylases Jmjd3 and Utx are required for T-cell differentiation. *Nat. Commun.* **6**, 8152 (2015).

35. Dobenecker, M.W. *et al.* Coupling of T cell receptor specificity to natural killer T cell development by bivalent histone H3 methylation. *J. Exp. Med.* **212**, 297–306 (2015).

36. Benlagha, K., Wei, D.G., Veiga, J., Teyton, L. & Bendelac, A. Characterization of the early stages of thymic NKT cell development. *J. Exp. Med.* **202**, 485–492 (2005).

37. Lee, Y.J., Holzapfel, K.L., Zhu, J., Jameson, S.C. & Hogquist, K.A. Steady-state production of IL-4 modulates immunity in mouse strains and is determined by lineage diversity of iNKT cells. *Nat. Immunol.* **14**, 1146–1154 (2013).

38. Gapin, L., Matsuda, J.L., Surh, C.D. & Kronenberg, M. NKT cells derive from double-positive thymocytes that are positively selected by CD1d. *Nat. Immunol.* **2**, 971–978 (2001).

39. Mao, A.P. *et al.* Multiple layers of transcriptional regulation by PLZF in NKT cell-cell development. *Proc. Natl. Acad. Sci. USA* **113**, 7602–7607 (2016).

40. Buenrostro, J.D., Giresi, P.G., Zaba, L.C., Chang, H.Y. & Greenleaf, W.J. Transposition of native chromatin for fast and sensitive epigenomic profiling of open chromatin, DNA-binding proteins and nucleosome position. *Nat. Methods* **10**, 1213–1218 (2013).

41. Pinello, L., Xu, J., Orkin, S.H. & Yuan, G.C. Analysis of chromatin-state plasticity identifies cell-type-specific regulators of H3K27me3 patterns. *Proc. Natl. Acad. Sci. USA* **111**, E344–E353 (2014).

42. Kanda, M. *et al.* Transcriptional regulator Bhlhe40 works as a cofactor of T-bet in the regulation of IFN-γ production in iNKT cells. *Proc. Natl. Acad. Sci. USA* **113**, E3394–E3402 (2016).

43. Engel, I. *et al.* Innate-like functions of natural killer T cell subsets result from highly divergent gene programs. *Nat. Immunol.* **17**, 728–739 (2016).

44. Williams, K.L. *et al.* BATF transgenic mice reveal a role for activator protein-1 in NKT cell development. *J. Immunol.* **170**, 2417–2426 (2003).

45. Jordan-Williams, K.L., Poston, S. & Taparowsky, E.J. BATF regulates the development and function of IL-17 producing iNKT cells. *BMC Immunol.* **14**, 16 (2013).

46. Lawson, V.J., Maurice, D., Silk, J.D., Cerundolo, V. & Weston, K. Aberrant selection and function of invariant NKT cells in the absence of AP-1 transcription factor Fra-2. *J. Immunol.* **183**, 2575–2584 (2009).

47. Thomsen, M.K. *et al.* JUNB/AP-1 controls IFN-γ during inflammatory liver disease. *J. Clin. Invest.* **123**, 5258–5268 (2013).

48. Miller, S.A., Mohn, S.E. & Weinmann, A.S. Jmjd3 and UTX play a demethylase-independent role in chromatin remodeling to regulate T-box family member-dependent gene expression. *Mol. Cell* **40**, 594–605 (2010).

49. Pereira, R.M. *et al.* Jarid2 is induced by TCR signalling and controls iNKT cell maturation. *Nat. Commun.* **5**, 4540 (2014).

50. Vahedi, G. *et al.* Super-enhancers delineate disease-associated regulatory nodes in T cells. *Nature* **520**, 558–562 (2015).

# ONLINE METHODS

**Experimental mice.** The targeting strategy for generating mice with *lox*P-flanked alleles encoding UTX (*Kdm6a*$^{f/f}$) or JMJD3 (*Kdm6b*$^{f/f}$) is shown in **Supplementary Figure 1**. *Jmjd3*$^{f/f}$ embryonic stem cells (ESCs) were generated by flanking exons 17 and 19 of the *Jmjd3* locus with *lox*P sites. These exons encode the catalytic JmjC domain. The sequence-verified targeting vector was linearized and electroporated into CJ9 ES cells (129sv background). Homologous recombination was assessed by Southern blot analysis by digesting genomic DNA with NheI (5′ probe) or KpnI (3′ probe), using specific external probes. *Kdm6a*$^{f/f}$ ESCs were obtained from EUCOMM. After sequence and genotype verification, karyotypically normal ESC clones were injected into blastocysts to generate chimera. Mice were backcrossed for at least ten generations to the C57BL/6 background. Additionally, UTX- and JMJD3-deficient animals were crossed to generate doubly deficient mice. UTX-sufficient (control) mice were derived from littermates. *Vav*-Cre mice (expressing Cre recombinase from the *Vav* allele), CD45.1-congenic mice and *Rag2*$^{-/-}$ mice were purchased from The Jackson Laboratory. JunB-KO (*Junb*$^{fl/fl}$MORE-Cre) mice were generated as previously described[51]. Sex- and age-matched animals between 8 and 12 weeks of age were used for experiments. To estimate proper number of animals, preliminary experiments were performed. Mice were allocated at random to experimental groups. Mouse studies were performed in a non-blinded fashion. The Institutional Animal Care and Use Committee (IACUC) of Boston Children's Hospital approved all animal experiments.

**Reagents.** Phorbol myristate acetate, ionomycin, FBS, and phosphate-buffered saline (PBS) were purchased from Sigma. Percoll was obtained from GE Healthcare Life Sciences. Viability Dyes (eFluor-780 and eFluor-450) were purchased from eBioscience. RPMI media 1640 and propidium iodide (PI) were purchased from Life Technologies. α-galactosylceramide (α-GalCer; PBS57) was obtained from Enzo Life Sciences. Brefeldin A was acquired from BioLegend.

**Antibodies.** For flow cytometry, cells were stained with following antibodies: anti-CD3 (145-2C11, 1:100), anti-CD8 (53-6.7, 1:100), anti-CD4 (GK1.5, 1:100), anti-CD24 (M1/69, 1:100), anti-CD45.1 (A20, 1:100), anti-CD45.2 (104, 1:100), anti-B220 (RA3-6B2, 1:100), anti-NKG2D (CX5, 1:100), anti-IL-2Rβ (TM-β1, 1:100), anti-CD94 (18d3, 1:100), anti-IFN-γ (XMG1.2, 1:100), anti-IL-4 (11B11, 1:100), and anti-T-bet (4B10, 1:100) were purchased from BioLegend. Anti-NK1.1 (PK136, 1:100), anti-TCR (H57-597, 1:100), anti-CD44 (IM7, 1:100), anti-IgG1 (A85-1, 1:100), anti-CD1d (1B1, 1:100), and anti-CD90.2 (53-2.1, 1:100) were obtained from BD Biosciences; anti-IL-17 (ebio17B7, 1:100) and anti-Rorγt (AFKJS-9, 1:100) were purchased from eBioscience; anti-PLZF (D-9, 1:500) was obtained from Santa Cruz Biotechnology; anti-CXCR3 (220803, 1:100) was purchased from R&D Systems; anti-S100a6 (EPNCIR121, 1:100) was obtained from Abcam; and anti-CD16/CD32 (2.4G2, 1 µg/ml) was acquired from Bio-Xcell (Malaysia).

**Flow cytometry.** Cells were stained with antibodies to surface makers (identified above) in flow cytometry buffer (PBS supplemented with 0.5% bovine serum albumin) on ice for 30 min. Subsequently, cells were washed and analyzed using a FACSCanto II flow cytometer (BD Biosciences). Propidium iodide was added just before flow cytometry analysis to exclude dead cells.

**Tetramer analysis.** For staining of *i*NKT cells, Alexa647- or phycoerythrin (PE)-conjugated α-GalCer-loaded CD1d tetramers (called simply 'CD1d tetramer' here) were obtained from the Tetramer Core Facility of the NIH. For blocking non-specific binding of immunoglobulin to Fc receptors, cells were incubated with anti-CD16/CD32 (identified above) in flow cytometry buffer for 10 min on ice. After incubation, cells were stained with fluorescence-conjugated CD1d tetramer and viability dye for 40 min on ice. To perform molecular studies, CD1d tetramer-positive cells were sorted using a FACSAria III (BD Biosciences).

**Intracellular staining for cytokines and transcription factors.** To stain cytokines intracellularly, cells were fixed and permeabilized with BD Cytofix/Cytoperm followed by staining with fluorescence-labeled antibodies to IFN-γ,

IL-4 or IL-17 (identified above) in Perm wash buffer (BD Biosciences). To analyze expression of transcription factors in *i*NKT cells, thymocytes were stained with fluorescence-conjugated CD1d tetramer, followed by fixation and permeabilization using the Foxp3/transcription factor staining buffer set (eBioscience). Subsequently, cells were incubated with purified anti-PLZF (identified above), followed by staining with fluorescence-labeled anti-mouse IgG1 (identified above). Thereafter, cells were stained with antibodies to T-bet and Rorγt (identified above).

**Isolation of liver lymphocytes.** To isolate liver mononuclear cells, livers were perfused with PBS through the portal vein, excised, and minced through a metal mesh. Tissue homogenates were collected in 50 ml of medium (RPMI supplemented with 2.5% FBS) and incubated for 15 min, before the supernatant was obtained. Cells were washed twice, suspended in medium containing 33% Percoll, and centrifuged at 500*g* at 20 °C without break. Thereafter, cell pellets were collected to perform further experiments.

**Measurement of immune responses to α-GalCer.** To test the function of thymic *i*NKT cells *in vitro*, CD8$^{-}$ thymocytes were selected using anti-CD8 conjugated to magnetic beads and MACS columns (Miltenyi Biotec), according to manufacturer's protocol. Subsequently, cells were stimulated with 50 ng/ml of phorbol myristate acetate and 5 µg/ml of ionomycin in culture medium (RPMI supplemented with 10% FBS) for 4 h. Brefeldin A was added for the final 2 h. To measure the *in vivo* responses to α-GalCer, mice were given injection of 250 µg of brefeldin A in 200 µl of PBS, followed 30 min later by intraperitoneal injection of 2 µg of α-GalCer in 200 µl of PBS. Mice were sacrificed 2 h after injection of α-GalCer, and livers were excised for the isolation of liver mononuclear cells and intracellular cytokine staining as described above.

**Mixed-bone-marrow-chimeric mice.** Bone marrow cells were isolated from the femurs and tibias of UTX-sufficient (control) B6.SJL (CD45.1$^{+}$) mice or UTX-KO (CD45.2$^{+}$) mice. T cells were depleted using biotinylated anti-CD90 (identified above), anti-biotin conjugated to magnetic beads, and MACS columns. *Rag2*$^{-/-}$ mice were irradiated with a cesium source (600 rads). Then, irradiated mice were given intravenous injection of a 1:1 mixture of bone marrow cells (2 × 10$^{6}$ per mouse) from UTX-KO mice and B6.SJL mice. Chimera were analyzed 10–12 weeks after bone-marrow-cell injection.

**Lentiviral transduction of bone marrow cells and UTX 'rescue' experiment.** Bone marrow cells from UTX-sufficient or UTX-KO mice were isolated and cultured with medium containing the cytokines IL-6, IL-3, IL-7 and SCF. After 24 h, cells were counted and spin-infected with lentivirus containing full-length UTX (pLVX-EF1a-IRES-mCherry-UTX-WT), or catalytically inactive UTX (pLVX-EF1a-IRES-mCherry-UTX-ED), and incubated for 3 h at 37 °C. After 24 h, cells were spin-infected again with the respective lentivirus and incubated for 3–4 h at 37 °C. Infected cells were collected and injected intravenously into irradiated (600 rads) *Rag2*$^{-/-}$ recipient mice.

**qRT-PCR.** Cells were sorted into TRI Reagent (Life Technologies), and total RNA was isolated according to the manufacturer's instructions with following modification: the aqueous phase containing total RNA was purified using the RNeasy plus kit (Qiagen). RNA was converted to cDNA with cDNA synthesis kit (Bio-Rad). qRT-PCR was performed with SYBR green master mix (Bio-Rad) on the Bio-Rad iCycler RT-PCR detection system. *Actb* was used as a housekeeping control. To calculate the relative change in expression (fold values), the 2$^{-\Delta\Delta CT}$ cycle threshold method was used. The following primer sequences were used: *Actb*, forward, 5′-TCCAGCCTTCCTTCTTGGGTATGGA-3′; *Actb*, reverse, 5′-CGCAGCTCAGTAACAGTCCGCC-3′; *Va14*, forward, 5′-GTCCTCAGTCCCTGGTTGTC-3′; *Ja18*, reverse, 5′-CAAAATGCAGCCTCCCTAAG-3′; *Tbx21*, forward, 5′-AGCAAGGACGGCGAATGTT-3′; *Tbx21*, reverse, 5′-GGGTGGACATATAAGCGGTTC-3′; *S100a6*, forward, 5′-GCTCACCATTGGCTCCAAGC-3′; *S100a6*, reverse, 5′-GGAAGGCGACATACTCCTGG-3′; *Klrd1*, forward, 5′-TCTAGGATCACTCGGTGGAGA-3′; *Klrd1*, reverse, 5′-CACTTGTCCAGGCAAACACAG-3′; *Klrk1*, forward, 5′-ACTCAGAGATGAGCAAATGCC-3′; *Klrk1*, reverse, 5′-CAGGTTGACTGGTAGTTAGTGC-3′; *Cxcr3*, forward, 5′-TACCTTGAGGTTAGTGAACGTCA-3′; *Cxcr3*, reverse, 5′-CGCTCTCGTTTTCCCCATAATC-3′; *Il2rb*,

forward, 5′-TGGAGCCTGTCCCTCTACG-3′; *Il2rb*, reverse, 5′-TCCACAT GCAAGAGACATTGG-3′; *Junb*, forward, 5′-CGACTACAAACTCCTGAA AC-3′; *Junb*, reverse, 5′-CTGTGTCTGATCCCTGAC-3′; *Utx*-delq, forward, 5′-GGTCACTTCAACCTCTTATTGG-3′; *Utx*-delq, reverse, 5′-CGACA TAAAGCACCTCCTGA-3′; *Jmjd3*-delq, forward, 5′-ATCCGAGGAACC AGACAGCACT-3′; *Jmjd3*-delq, reverse, 5′-GAGCATGTTGCCTGTGG ATG-3′; *Il18r1*, forward: 5′-ACTTTTGCTGTGGAGACGTTAC-3′; *Il18r1*, reverse: 5′-CCGGCTTTTCTCTATCAGTGAAT-3′; *Il12rb1*, forward: 5′-ATGGCTGCTGCGTTGAGAA-3′; *Il12rb1*, reverse: 5′-AGCACTCATAG TCTGTCTTGGA-3′; *Eya2*, forward: 5′- ACCGCTGGGCTCTATCAAG-3′; and *Eya2*, reverse: 5′-GGTAGGACGGATAATCCTGGTG-3′.

**Gene expression microarray.** Control or UTX-KO thymic *i*NKT cells were sorted into TRI Reagent (Life Technologies), and total RNA was isolated as described above. RNA was reverse transcribed and amplified using Ovation Pico RNA Amplification System V2 (NuGEN), biotin-labeled (Encore Biotin Module, NuGEN), and hybridized to Affymetrix mouse 430A 2.0 arrays. Affymetrix CEL files were normalized using the Robust Multi-array Average (RMA) method[52], and batch effects were removed using ComBat[53]. Differentially expressed genes were detected by lmFit function in the limma package[54]. Gene-set–enrichment analysis (http://www.broadinstitute.org/gsea/index.jsp) was conducted on a pre-ranked list of genes expressed differentially in UTX-KO *i*NKT cells relative to their expression in control *i*NKT cells. Furthermore, analysis with the Genomic Regions Enrichment of Annotations Tool (GREAT; http://bejerano.stanford.edu/great/public/html/splash.php) was performed on differentially expressed genes in order to identify their functional annotations[55].

**Genome-wide ChIP-Seq analysis.** ChIP-Seq for histone marks H3K4me3 and H3K27me3 was performed as described previously[56]. $1 \times 10^5$ flow-cytometry-sorted thymic *i*NKT cells were fixed with 1% formaldehyde (EMS) for 5 min at 25 °C. Cells were lysed in 120 µl of ChIP buffer (0.5% SDS, 50 mM Tris, pH 8, 10 mM EDTA, 1 × complete protease inhibitor cocktail, Roche) and were sonicated with an E210 Ultrasonicator (Covaris) in microtubes (Covaris) with the following sonication conditions: intensity, 5; duty cycle, 10%; 200 cycles per burst for 60 s and repeated six times. Sonicated chromatin was collected and diluted with four parts of ChIP dilution buffer (1.25% Triton X-100, 12.5 mM Tris, pH 8, 187.5 mM NaCl, 1× complete protease inhibitor cocktail). Input samples were collected and stored at −20 °C. Dynabeads Protein G (Life Technologies) coupled to specific antibodies were used for overnight immunoprecipitation using anti-H3K4me3 (ab8580, Abcam, 5 µg per ChIP) or anti-H3K27me3 (07-449, Millipore, 5 µg per ChIP). Subsequently, samples were washed and the ChIP immune complexes were eluted from the beads twice, using elution buffer (1% SDS and 0.1 M NaHCO$_3$) under constant agitation for 30 min. Samples were pooled and incubated overnight at 65 °C for reversal of the formaldehyde crosslinks. The samples were then treated for 2 h at 37 °C with 200 µg RNase A (Qiagen) and 40 µg proteinase K (Life Technologies). ChIP DNA fragments were purified with a MinElute Reaction Cleanup kit (Qiagen). ChIP DNA was prepared for high-throughput Illumina sequencing with a NEBNext ChIP-Seq Library Prep Master Mix Set for Illumina kit (New England BioLabs) and NEBNext Multiplex Oligos for Illumina (Index Primers 1–12) according to a modified manufacturer's protocol. For each ChIP, the ends of DNA fragments were repaired, dA-tailed and ligated to Illumina adaptors according to the kit instructions. DNA fragments 150–600 bp in length were then selected with Pippin Prep 2% Agarose Gel Cassettes and the Pippin Prep DNA Size Selection System (Sage Science). After each step, DNA was purified with a MinElute Reaction Cleanup Kit or a QIAquick PCR Purification Kit (Qiagen). The DNA obtained by ChIP was then amplified by 15 cycles of PCR with NEBNext Multiplex Oligos. Amplified DNA was purified with DNA to Agencourt AMPure XP beads (Beckman Coulter) at a ratio of 1:1. The 'multiplexed' DNA libraries were sequenced on the Illumina HiSeq2000. Chip-Seq raw reads were aligned using the Bowtie2 aligner[57] on the mouse genome assembly mm9 (National Center for Biotechnology Information), and peaks were called using MACS2[58] with the default parameter. To compare the average profiles, the different tracks were down-sampled to the same number of reads, and duplicate reads were removed using the PICARD tool (http://broadinstitute.github.io/picard/). To assess the significance of differences between two average profiles in a given region, we computed empirically, using 100,000 permutations, the distribution of the differences between two profiles using random assignment.

**Cluster analysis of H3K27me3 and H3K4me3.** Cluster analysis was performed on the promoter regions of various sets of genes. The promoter region was defined as transcription start site (TSS) −2 kb and TSS +2 kb. The number of clusters was determined using a Silhouette metric[59], and K-means was performed thereafter using the Euclidean distance.

**UTX and JunB ChIP-PCR.** ChIP was performed as described with modifications[56]. $2 \times 10^6$ flow-cytometry-sorted *i*NKT cells were fixed with 1% formaldehyde (EMS) for 5 min at 25 °C. Anti-UTX (Bethyl, A302-374, 5 µg per ChIP) and anti-JunB (CST, C37F9, 5 µg per ChIP) were incubated with beads for 3–5 h before incubation with sonicated chromatin overnight. ChIP DNA was purified and quantified by real-time PCR using the iQ SYBR Green Supermix (Bio-Rad). The following primer sequences were used: *S100a6* promoter, forward, 5′-GAAGGTTCAGCACACAAGCC-3′; *S100a6* promoter, reverse, 5′-CCCAAAGGAGACCAGTGCAA-3′; *Il2rb* promoter, forward, 5′-TAAGATCTCCTCCTACGCCCA-3′; *Il2rb* promoter, reverse, 5′-ATGTGTGAGATGTAGCGGGG-3′; *Tbx21* promoter, forward, 5′-TGAA ACTTCACTGGAGCGGG-3′; *Tbx21* promoter, reverse, 5′-TTCATAAAGCC ACAGCAAAGGC-3′; *Klrd1* promoter, forward, 5′-TGCATCTGTGTC CCACCAAC-3′; *Klrd1* promoter, reverse, 5′-CCAAGGATGGTGCAGAGAT GT-3′; *Actb* promoter, forward, 5′-TGCCCCATTCAATGTCTCGG-3′; and *Actb* promoter, reverse, 5′-CCACACAAATAGGGTCCGGG-3′.

**Immunoprecipitation and immunoblot analysis.** Cell lysates were incubated with 5 µg anti-UTX (Bethyl, A302-374) or the control antibody anti-rabbit IgG (Santa Cruz, sc-2027) overnight at 4 °C followed by 2 h of incubation with Dynabeads Protein G for immunoprecipitation. Protein complexes bound to antibody and beads were washed five times and eluted with Laemmli sample buffer. Samples were resolved by SDS-PAGE. Protein interactions were analyzed by immunoblot with the primary antibodies anti-PLZF (R&D, AF2944, 1:500) or anti-JunB (CST, C37F9, 1:500), and the secondary antibody goat anti-rabbit IgG-HRP (Santa Cruz, sc-2030, 1:5,000), followed by visualization using the Western Lightning Plus ECL detection kit (PerkinElmer).

**Transcription factor (TF) target motif enrichment using Haystack.** To identify potential TFs that mediate the observed gene expression changes, we scanned gene promoters for enriched TF motifs using the *haystack_motifs* utility from the Haystack Pipeline (https://github.com/lucapinello/Haystack)[41]. For analysis, we used the default parameters for the mouse genome: the mm9 genome assembly and the JASPAR motif database[60]. Subsequently, to remove potential false positives, we further integrated gene-expression data to assess their specificity and concordance with gene-expression changes. In particular, we filtered TF motifs on the basis of visual exploration of the ratio of the expression of TFs and their targets in control cells to that in UTX-KO, using the *haystack_tf_activity_plane* utility.

**Super-enhancer analysis.** To call super-enhancers, we used the ROSE algorithm, version 0.1 (https://bitbucket.org/young_computation/rose)[14]. In particular, we first considered as enhancers peaks of H3K27ac obtained by the software MACS2, and then called ROSE with default parameters to define the super-enhancers. Using these settings, peaks closer than 12.5 kb were stitched together and then ranked based of the H3K27ac intensity. To assign super-enhancers to genes, we used again ROSE with default settings.

**Genome-wide ATAC-Seq.** ATAC-Seq was performed as previously described[42]. Control and UTX-KO thymic *i*NKT cells were sorted by flow cytometry and were lysed in lysis buffer containing 10 mM Tris-HCl pH 7.4, 10 mM NaCl, 3 mM MgCl$_2$, 0.1% IGEPAL CA-360. The transposition reaction was carried out for 45 min using the Illumina Nextera DNA preparation kit (FC-121-1030). DNA was purified using the Qiagen MinElute PCR purification kit. Subsequently, library amplification was performed using Nextera primers and NEBNext high-fidelity PCR master mix. Quantitative PCR side reaction was done to determine optimum library amplification to diminish GC and

size bias in the library. The amplified library was purified using the Qiagen PCR purification kit and sequenced on the Illumina Hi-Seq 2500. Paired reads were aligned to the reference genome using Bowtie2 in paired end mode and with the parameter -X2000 (fragments up to 2kb). ATAC-Seq peaks were called using MACS2 with the following parameters: macs2 callpeak –nomodel –shift -100 –extsize 200. Super-enhancers more accessible in control cells were defined as control super-enhancer regions containing unique control ATAC-Seq peaks, while super-enhancers less accessible in control cells were defined as control super-enhancer regions containing unique KO ATAC-Seq peaks.

**Integrative analysis of SE regions, ATAC-Seq, H3K27me3 and gene expression.** To study the potential connection between the level of H3K27me3 and chromatin accessibility profiled by ATAC-Seq, we used the defined super-enhancers based on the unique ATAC-Seq peaks in control or UTX-KO and profiled the average abundance of H3K27me3 reads per million (RPM) in those regions. As a control set, we used random regions in the genome. To correlate chromatin accessibility in super-enhancers with gene expression, we used the average gene expression of the genes mapped with the ROSE pipeline in each group (closest genes and overlapping genes). As control sets, we used all the genes and the genes mapped to all the UTX-sufficient super-enhancers in iNKT cells.

**Statistical analysis.** Data are presented as mean ± standard error or standard deviation. All samples represent independent experiments with biological replicates. Sample size was determined based on the results of preliminary experiments. No blinding was applied in this study. The two-tailed unpaired $t$-test, Mann-Whitney $U$-test and one-way ANOVA with post multiple-comparisons were applied as indicated, and the $P$ values are shown for each figure. If not otherwise indicated, the $P$ value was not statistically significant ($P > 0.05$). All statistical analyses for animal studies were calculated using Prism software (GraphPad).

**Data availability.** Data that support the findings of this study have been deposited in the Gene Expression Omnibus (GEO) database under accession numbers GSE84238 and GSE84015.

51. Passegué, E., Wagner, E.F. & Weissman, I.L. JunB deficiency leads to a myeloproliferative disorder arising from hematopoietic stem cells. *Cell* **119**, 431–443 (2004).
52. Irizarry, R.A. *et al.* Exploration, normalization, and summaries of high density oligonucleotide array probe level data. *Biostatistics* **4**, 249–264 (2003).
53. Johnson, W.E., Li, C. & Rabinovic, A. Adjusting batch effects in microarray expression data using empirical Bayes methods. *Biostatistics* **8**, 118–127 (2007).
54. Smyth, G.K. Linear models and empirical bayes methods for assessing differential expression in microarray experiments. *Stat. Appl. Genet. Mol. Biol.* **3**, Article3 (2004).
55. McLean, C.Y. *et al.* GREAT improves functional interpretation of cis-regulatory regions. *Nat. Biotechnol.* **28**, 495–501 (2010).
56. Kurachi, M. *et al.* The transcription factor BATF operates as an essential differentiation checkpoint in early effector CD8+ T cells. *Nat. Immunol.* **15**, 373–383 (2014).
57. Langmead, B. & Salzberg, S.L. Fast gapped-read alignment with Bowtie 2. *Nat. Methods* **9**, 357–359 (2012).
58. Zhang, Y. *et al.* Model-based analysis of ChIP-Seq (MACS). *Genome Biol.* **9**, R137 (2008).
59. Rousseeuw, P.J. Silhouettes: A graphical aid to the interpretation and validation of cluster analysis. *J. Comput. Appl. Math.* **20**, 53–65 (1987).
60. Mathelier, A. *et al.* JASPAR 2014: an extensively expanded and updated open-access database of transcription factor binding profiles. *Nucleic Acids Res.* **42**, D142–D147 (2014).